# 國 立 清 華 大 學

## 博 士 論 文

# 利用非線性光混頻產生高效率兆赫波

# High Efficiency THz-wave Generation from Nonlinear Frequency Mixing


系所別　光電工程研究所

學號姓名　938107　王寵棟（Tsong-Dong Wang）

指導教授　黃衍介　博士（Dr. Yen-Chieh Huang）



中華民國九十八年七月

## Abstract

In the past few years, widely tunable terahertz (THz) generation from parametric frequency mixing in nonlinear optical crystals has drawn much attention. The scope of the interest on and application of THz wave includes molecular science, solid-state physics, biomedical applications, diagnostics, and ultra-high speed optical communications, among many others. In this thesis, we generated coherent THz waves from lithium niobate by two novel schemes: the non-collinearly phase-matched THz-wave parametric generation in waveguide-type lithium niobate ($LiNbO_3$) and the collinearly phase-matched THz-wave difference-frequency generation in periodically poled lithium niobate (PPLN).

In the non-collinearly phase-matched scheme, we observed a parametric-generation efficiency of 1.61% from 1064 nm to 1071 nm and 162 μm in a 0.5 mm thick, 45 mm long z-cut congruent lithium-niobate waveguide with a pump energy of 2.2 mJ and a pump pulse width of 5.8 ns. We also measured an ultra-low-threshold, narrow-line THz-wave parametric oscillator with an intra-cavity grazing-incidence grating and a 1 mm thick, 45 mm long lithium-niobate planar waveguide. When pumped by an actively Q-switched Nd:YAG laser, the threshold energy and intensity of the parametric oscillator were about 2.2 mJ and 70 $MW/cm^2$, respectively. The linewidths of the output THz wave were 12 GHz and 134 GHz with and without the intra-cavity grating, respectively. The energy conversion efficiency, the pump threshold, and the THz linewidth are the highest, lowest, and narrowest among all the reported values for similar devices.

In the collinearly phase-matched scheme, we first generated a dual-wavelength 1.5 μm laser with a 17 μJ energy (peak power 45 kW) from an optical parametric amplification system as the pump source. We then generated a THz-wave in the wavelength range of 190~210 μm and 457~507 μm from a forward and backward difference frequency generator (DFG), respectively, by using a 3.2 cm long multi-grating PPLN crystal. The grating period of the PPLN crystal varied from 63 to 70 μm in 1 μm increments. The extraordinary refractive index of $LiNbO_3$ in the THz-wave range was precisely deduced from the quasi-phase-matching condition of the difference frequency generations. We estimated that about 0.37 pJ and 0.056 pJ

energies of the forward and backward THz waves, respectively, were generated in the PPLN crystal. My work is the first demonstration of forward and backward THz-wave generations from collinearly phase-matched difference frequency mixing in PPLN.

# 中文摘要

過去幾年中，以非線性晶體作為增益介質，利用非線性光學光參數方式來產生兆赫波幅射，這種方式吸引很多人的注意。綜觀兆赫波方面的研究與應用，包含：分子科學、固態物理、生物醫學、非破壞性診斷、與超快光通訊等。在我們實驗室裡，利用非線性晶體鈮酸鋰($LiNbO_3$)， 使用兩種基本方式實現了高同調性並且波長可調的兆赫波幅射在此晶體中，第一種方式為：利用非同向性相位匹配兆赫波參數產生與震盪方式在鈮酸鋰($LiNbO_3$)晶體中；另一種方式為：使用同向性準相位匹配兆赫波光差頻產生方式在週期性極化鈮酸鋰(PPLN)晶體中。

在非同向性相位匹配架構中，我們觀察到當鈮酸鋰只有 0.5mm 厚度時(其長度為 45mm、z-cut 鈮酸鋰兆赫波波導)，在泵浦光(其能量為 2.2mJ、脈衝寬度為 5.8ns)波長為 1064nm 轉換到 1071nm 跟 162μm 的光參數產生轉換效率高達 1.61%，這是第一次我們由實驗證明有如此高的轉換效率是因為兆赫波在此晶體中受到光波導效應而提高。

另一方面，在一個 intra-cavity grazing incident grating 幫助下，我們同時也觀察到超低閾值、窄頻兆赫波參數震盪器來產生兆赫波，其增益晶體為一片厚度 1mm、長度 45mm 兆赫波光波導的鈮酸鋰晶體中。本架構是由主動式 Q 開關雷射當泵浦光供給能量來產生光參數轉換，在此震盪器中我們發現閾值(threshold)只需 2.2mJ 的能量(或是強度 70MW/$cm^2$)。更近一步我們發現，在有或者是沒有 intra-cavity grazing incident grating 幫助下，震盪器中兆赫波的線寬分別為 12GHz 與 134GHz，這表示我們使用 grating 可以大大降低兆赫波的頻寬，頻寬的降低對光譜學上可以得到很好的應用。藉由此實驗架構跟同類型的實驗架構相比較，我們所產生的兆赫波參數震盪器的閾值(threshold)是最小的，而兆赫波的頻寬是最窄的。

在同向性架構中，首先藉由光參數放大器系統中產生雙波長為 1.5μm 附近的泵浦光源，此雙波長雷射光擁有總能量為 17μJ (總峰值功率為 45KW)，然後利用此雙波長雷射產生光參數雷射差頻正向與反向兆赫波，其波長分別是 190~210μm 與 457~507μm，此時使用的晶體為 3.2cm 長的週期性極化酸鋰(PPLN)晶體。此

晶體的極化週期在每 1μm 變化下從 63μm 到 70μm。並且鈮酸鋰晶體在兆赫波段的異常折射率也藉由在準相位匹配條件下，由雷射差頻方式精準的量測出來。並且我們預估分別有 0.37pJ 與 0.056pJ 在正向與反向兆赫波能量。在這實驗中，我們第一次在週期性極化酸鋰晶體中利用雷射光差頻產生器實現了三波同向的正向與反向兆赫波。

Acknowledgements

My deepest heartfelt gratitude first goes to my advisor—Prof. Yen-Chieh Huang. He is a diligent researcher, devoting much time and effort to this field. More importantly, he is a respectful mentor, who is always generous in offering me all kinds of valuable help. Without his boundless encouragement, patient guidance, and endless tolerance, I could not have gotten this far. I would also like to convey my sincere gratitude for his repeated revisions of the manuscripts of my thesis.

Next, I would like to express my appreciation to my committee members—Prof. Chi-Kuang Sun, Prof. Yen-Hung Chen, Prof. Fan-Yi Lin and Prof. Ja-Yu Lu, for their valuable and constructive suggestions with regard to the present study. I am grateful to have their warm encouragement and advice in regard to my oral defense. Special thanks go to Dr. An-Chung Chiang, Dr. Yen-Yin Lin, Dr. Shou-Tai Lin, and Dr. Yuan-Yao Lin, for their timely assistance and supportive friendship during the execution of the research. Without their help, this research would not have been possible. I am also thankful from the bottom of my heart for all the participants in this study.

In addition, I am profoundly indebted to my family for their wholehearted love and care, which helped me overcome every obstacle in my life. Their unfailing faith in me turns out to be the most powerful force, motivating me to pursue my dream and future without hesitation. Their unconditional love has enriched my life immeasurably.

A lot of thanks go to my wife, Yu-Fang Chou, for the boundless love, care, and tolerance she has shown me. I thank her for having incredible confidence in me and guiding me to look for the positive side of every challenge. I am grateful to have her share in every delightful and joyful moment.

Finally, I owe sincere thanks to all my research group members who consistently provide me with spiritual support and help whenever I need them. The time we spend together will always be the most precious memories. They were of great help during many difficult times.

## Table of Contents

## List of Figures

## List of Tables

# Chapter 1 Introduction

## 1-1 Motivation

Terahertz (THz) radiation, which is in the frequency gap between the infrared and microwaves, has been widely studied in various research fields such as molecular spectroscopy, noninvasive imaging, homeland security [1, 2, 3, 4], and many others. So far, THz radiation has been regarded as "safe radiation," especially when compared with X-rays. Compared with visible light, THz radiation can penetrate better through some materials such as cardboard, clothes, paper, leather, plastic, wood, and so on. However, it cannot penetrate metal and could be strongly absorbed by water. When a THz wave passes through a material it interacts with the material via mechanisms different from that for a visible light. For example, THz radiation is a powerful tool that can help investigate the slow vibration and rotation modes of a large molecule.

In the past few decades, generating THz wave by optical rectification in a nonlinear optical material and optically gated current switching in a photoconductive material has been studied extensively [5, 6]. These two techniques are efficient means of producing incoherent, broadband THz radiations. There are many approaches to generate coherent THz waves. For example, free electron laser can generate high-power broadly tunable THz radiations. However, the large size and high cost of the free electron lasers has restricted their use by a limited number of researchers [7]. On the other hand, there is a potential way to develop a simple, convenient, coherent, and tunable THz wave source by using nonlinear frequency mixing in lithium niobate ($LiNbO_3$). This approach is based on tunable light scattering from both electronic and vibrational nonlinear dipoles of the material. In particular, THz parametric generation from $LiNbO_3$ crystals pioneered by Pantell [8] has been greatly improved by H. Ito [9, 10] in the past 15 years. In this thesis, we demonstrate coherent THz radiation from $LiNbO_3$ via two novel approaches: the non-collinearly phase-matched THz-wave parametric oscillator (TPO) in $LiNbO_3$ waveguides and the collinearly phase-matched THz-wave difference-frequency generator (DFG) in periodically-poled $LiNbO_3$

(PPLN).

The major difference between our non-collinear THz-wave parametric generator (TPG) and that of Ito is that we take advantage of guiding of the THz wave in our thin $LiNbO_3$ crystal to enhance the parametric conversion efficiency. We also take advantage of the grazing incidence configuration of an intracavity grating in the TPO to reduce the generated THz-wave linewidth.

Our collinear THz-wave DFG permits a long parametric gain length and offers a possibility of efficiently generating tunable THz radiation. The collinear THz-wave DFG is based on the quasi-phase-matching (QPM) technique [11]. The advantage of the QPM technique is that it permits the choice of the highest nonlinear coefficient in a nonlinear optical crystal for collinear wave mixing, leading to the demonstration of many low-threshold and high-efficiency lasers. PPLN has attracted much attention because of its large nonlinear optical coefficient $d_{33}$=27pm/V, high optical quality, and available large crystal size. In the collinear THz-wave DFG configuration, one can study not only the forward phase matched nonlinear frequency mixing process but also the backward phased matched one. Since S. E. Harris's development of the theory of optical parametric oscillator (OPO) [12], there has been no demonstration of THz-wave backward OPO so far. Recently, however, this scheme has been successfully demonstrated in mid-infrared spectrum [13]. By using the QPM technique, it could be possible to realize backward OPO in the THz region.

In summary, the focus of my thesis is on the development of compact, coherent, and tunable THz-wave generators.

## 1-2 THz-wave Generation Using Polariton Scattering in Polar Crystals

A polariton is a quantum of the coupled phonon-photon transverse wave field. A polariton can be excited by using a sufficient strong pump input in polar crystals such as $LiNbO_3$, $LiTaO_3$, and GaP. THz-wave generation results from polariton scattering, which involves second- and third-order nonlinear processes. $LiNbO_3$, a polar crystal, has a transverse optical (TO) phonon mode (248 $cm^{-1}$) called the A1-symmetry mode; therefore, the THz parametric gain results from the coupling between the electronic and ionic nonlinearity. With regard to generating THz-wave through polariton

scattering in $LiNbO_3$, ionic nonlinearity has been reported to account for 80% the total effective nonlinear coefficient [14]. Therefore, $LiNbO_3$ is one of the most suitable crystals to generate THz wave efficiently through laser pumped nonlinear frequency mixing because of its large effective nonlinear coefficient and its wide transparent range covered by the laser spectrum (0.4 μm -5.5 μm).

The principle of parametric non-collinear THz-wave generation is shown in Fig. 1-1 and explained as follows. When the polaritons are in the non-resonant frequency range (resonant frequency: $\omega_{TO}$), their behavior is like that of photons. Hence, a THz photon $(\omega_{THz})$ and an optical-frequency signal photon $(\omega_s)$ can be generated by a pump photon $(\omega_p)$ under the energy and momentum conservation laws, $\omega_p = \omega_s + \omega_{THz}$ $\left( or \quad \frac{1}{\lambda_p} = \frac{1}{\lambda_s} + \frac{1}{\lambda_{THz}} \right)$ and $\vec{k}_p = \vec{k}_s + \vec{k}_{THz}$, where the subscripts p, s, and THz, denote the quantities associated with the pump, signal, and THz waves, respectively; $\omega$ is the angular frequency; and $\vec{k}$ is the wave vector of the mixing waves. To satisfy $\vec{k}_p = \vec{k}_s + \vec{k}_{THz}$, the mixing waves could be collinearly or non-collinearly aligned according to the dispersion characteristics of the material.

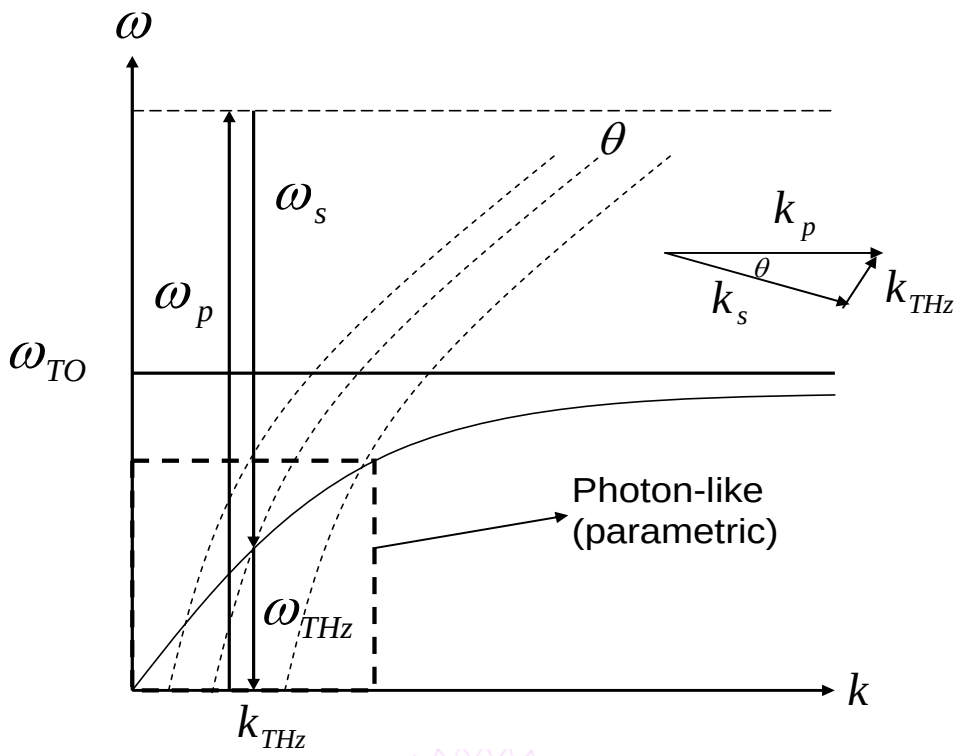


**Fig. 1-1** Dispersion curve of polaritons. A polariton can be excited by the coupling of a photon and a transverse optical phonon ( $\omega_{TO}$ , resonant frequency) with an intense pump laser. Therefore, the behavior of polaritons in the low-energy range is like photons at the THz frequency region (non-resonant frequency region). The inset indicates the non-collinear phase-matching condition (momentum conservation law).

## 1-3 Optical Properties of Lithium Niobate in THz-frequency Region

### *Nonlinear coefficients in the THz-frequency range*

The dielectric material $LiNbO_3$ contains four resonant modes corresponding to the different lattice vibration modes (transverse optical phonon modes). These modes cause the ionic dipole moment ( $d_{Qj}$ term) to contribute ~80% to the total 2nd-order nonlinear susceptbility. As a result, $\chi_P$ , denoting the total nonlinear susceptibility in a parametric process, is expressed as [14]

$$\chi_P = d_E + \sum_j \frac{S_j \nu_{oj}^2}{\nu_{oj}^{\ 2} - \nu^2} \cdot d_{Qj} \tag{1-1}$$

where $\nu_{oj}$ and $S_j$ are the eigenfrequency and oscillator strength of the A1-symmetry phonon modes, respectively. The coefficients $d_E = (16\pi d_{33})$ (second-order

nonlinearity) and $d_{Qj}$ (third-order nonlinearity) denote the nonlinear coefficients arising from electronic and ionic dipoles, respectively. By convention, the effective nonlinear coefficient can be expressed as $d_{eff} = \frac{\chi_P}{16\pi}$ (see Fig. 1-2). (All the susceptibility parameters listed are in Table 1-1 in CGS units. Note that to convert $d_{eff}$ into the MKS, one multiplies it by $\frac{4\pi}{3\times10^4}$ to obtain $d_{eff}$ in units of m/V [15].

**Table 1-1.** Properties of A1-symmtry modes in $LiNbO_3$ characterized by infrared reflectivity measurements [16]. Mode frequency is defined to be the inverse of the wavelength $\left(1/\lambda\ cm^{-1}\right)$. The coefficient $d_{Qj}$ (third-order nonlinearity) denotes the nonlinear coefficients arising from ionic dipoles.

| Mode frequency $\nu_{oj}$ ($cm^{-1}$) | Oscillator strength $S_j$ | Linewidth $\Gamma_j$ ($cm^{-1}$) | Nonlinear coefficient $d_{Qj}$ $\times10^{-6}$ (esu) |
|---|---|---|---|
| 248 | 16.0 | 21 | +1.2 |
| 274 | 1.0 | 14 | -2.3 |
| 307 | 0.16 | 25 | -2.8 |
| 628 | 2.55 | 34 | +1.8 |
| $\varepsilon_\infty = 4.6$ | | $d_e = 5.25\times10^{-6}\,esu$ | |

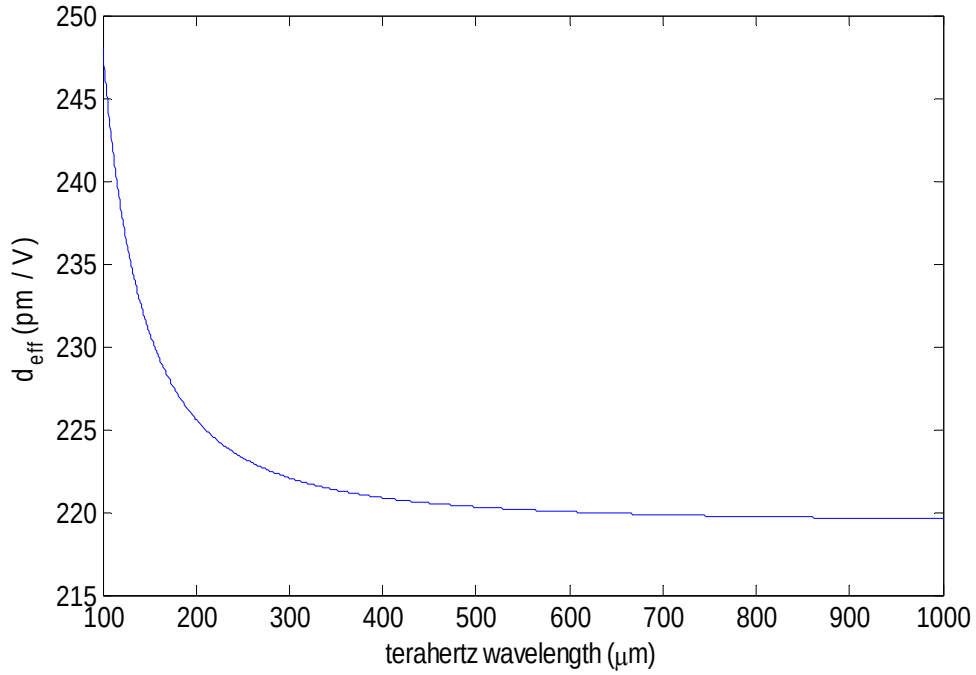


**Fig. 1-2** Due to the contribution of the ionic dipole moment, the effective nonlinear coefficient $d_{eff}$ is ~ 230 pm/V in THz-frequency region.

***Refractive indices and absorption coefficients in the THz-frequency range***

The linear susceptibility in the THz-frequency range is also the sum of the contributions from these resonant TO phonon modes. This is manifested in the frequency dependence of the absorption coefficient and refractive index. The linear susceptibility of a polar material in the THz-wavelength range can be described as [14]

$$\varepsilon(\omega_{THz}) = \left( \varepsilon_{\infty} + \sum_{j} \frac{S_j \nu_{oj}^2}{\nu_{oj}^2 - \nu^2 - i\nu\Gamma_j} \right) \tag{1-2}$$

where $\nu_{oj}$, $S_j$, and $\Gamma_j$ are the eigenfrequency, oscillator strength, and damping linewidth of the A1-symmetry phonon modes, respectively. The corresponding refractive indices and absorption coefficients are shown in Fig. 1-3. It is seen that, in the THz region, the extraordinary refractive indices are about 5.3. However, the absorption coefficient strongly depends on frequency (ranging from ~1 $cm^{-1}$ to ~100 $cm^{-1}$ between 0.3 and 3 THz-frequency range).

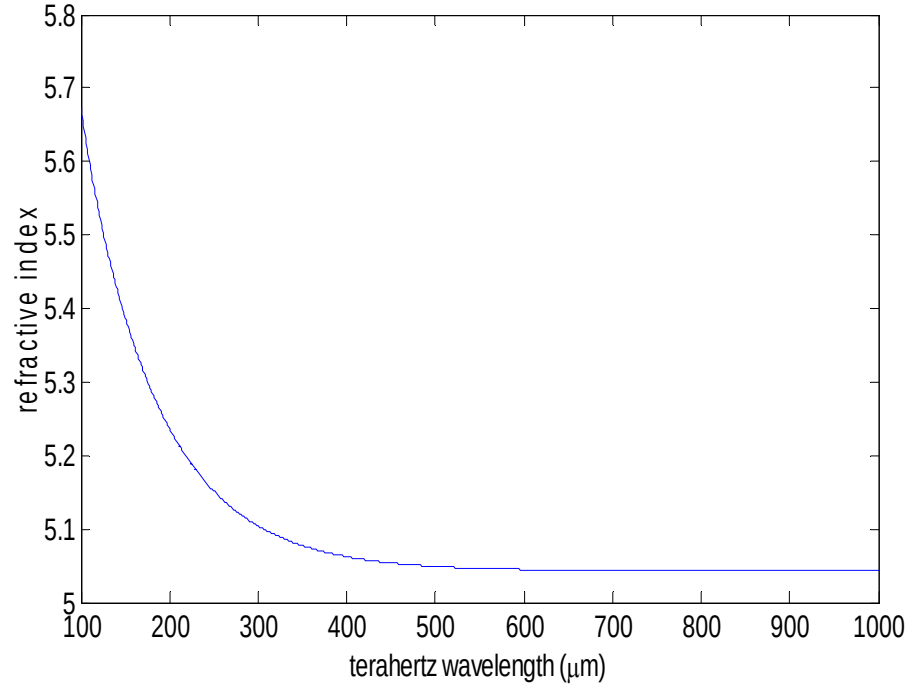


(a)

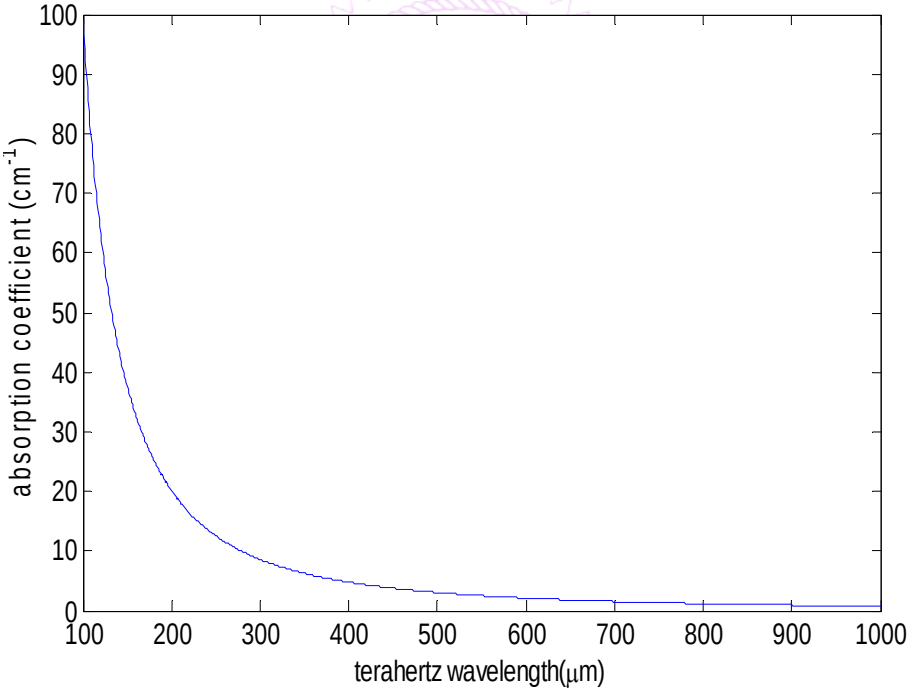


(b)

**Fig. 1-3** (a) The THz extraordinary refractive index deduced from Eq. (1-2), with $n(\omega_{THz}) = \mathrm{Re}\left(\sqrt{\varepsilon(\omega_{THz})}\right)$. (b) The absorption coefficients defined by $\alpha_{THz}(\omega_{THz}) = \frac{2\omega}{c_o}\mathrm{Im}\left(\sqrt{\varepsilon(\omega_{THz})}\right)$ and calculated from Eq. (1-2), where $c_o$ is the speed of light in vacuum.

## 1-4 Non-collinear Phase-matched THz-wave Generation

***Theory of THz-wave parametric gain***

In the stimulated scattering polariton, the couple wave equations for $E_{THz}$, $E_s$, and $E_p$ can be expressed by Equation 1-3 [14]. The parametric gain for the signal and THz waves are derived from solving the couple-wave equations in CGS unit.

$$\begin{aligned}
&\left(\nabla^2+\frac{\omega_{THz}^2}{c_o^2}\varepsilon_{THz}\right)E_{THz}=-\frac{\omega_{THz}^2}{c_o^2}\chi_P E_p E_s^* \\
&\left[\nabla^2+\frac{\omega_s^2}{c_o^2}\left(\varepsilon_s+\chi_R\left|E_p\right|^2\right)\right]E_s=-\frac{\omega_s^2}{c_o^2}\chi_P E_p E_{THz}^* \\
&\left[\nabla^2+\frac{\omega_p^2}{c_o^2}\left(\varepsilon_p+\chi_R\left|E_s\right|^2\right)\right]E_p=-\frac{\omega_p^2}{c_o^2}\chi_P E_s E_{THz}
\end{aligned} \tag{1-3}$$

where $\omega_{THz,s,p}$ denote the angular frequency of the THz, signal, and pump waves. $\varepsilon_{THz,s,p}$ represent the permittivity of the THz, signal, and pump waves in the $LiNbO_3$ material.

The nonlinear susceptibilities $\chi_P$ and $\chi_R$ denote the parametric and Raman processes, respectively, and they can be expressed as [14]

$$\begin{aligned}
\chi_P &= d_E+\sum_j \frac{S_j\nu_{oj}^2}{\nu_{oj}^{\ 2}-\nu^2}\cdot d_{Qj} \\
\chi_R &= \sum_j \frac{S_j\nu_{oj}^2}{\nu_{oj}^2-\nu^2-i\nu\Gamma_j}\cdot d_{Qj}^2
\end{aligned} \tag{1-4}$$

Assuming a steady state and no pump depletion, Equations 1-3 can be solved by using the plane wave approach. Therefore, the analytical solutions of the exponential gain coefficient for THz and signal waves are [14]

$$g_{THz}=g_s\cos\phi=\frac{\alpha_{THz}}{2}\left(\sqrt{1+16\cos\phi\left(\frac{\Gamma}{\alpha_{THz}}\right)^2}-1\right) \tag{1-5}$$

where $\phi$ is the non-collinear phase-matching angle between the pump and the THz

waves. $\Gamma$ ($\Gamma^2 = \frac{2\omega_s \omega_{THz} d_{eff}^2 I_p}{\varepsilon_0 n_p n_s n_{THz} c_0^3}$) is the power-lossless gain coefficient; $\alpha_{THz}$ is the power absorption coefficient in the THz-wave region. Figure 1-4 shows the THz-wave gain coefficient $g_{THz}$ with two different pump intensities, 70 MW/cm$^2$ and 140 MW/cm$^2$ at 1064 nm in a $LiNbO_3$ crystal. This indicates the gain is in the order of several cm$^{-1}$ with a high peak power pumping.

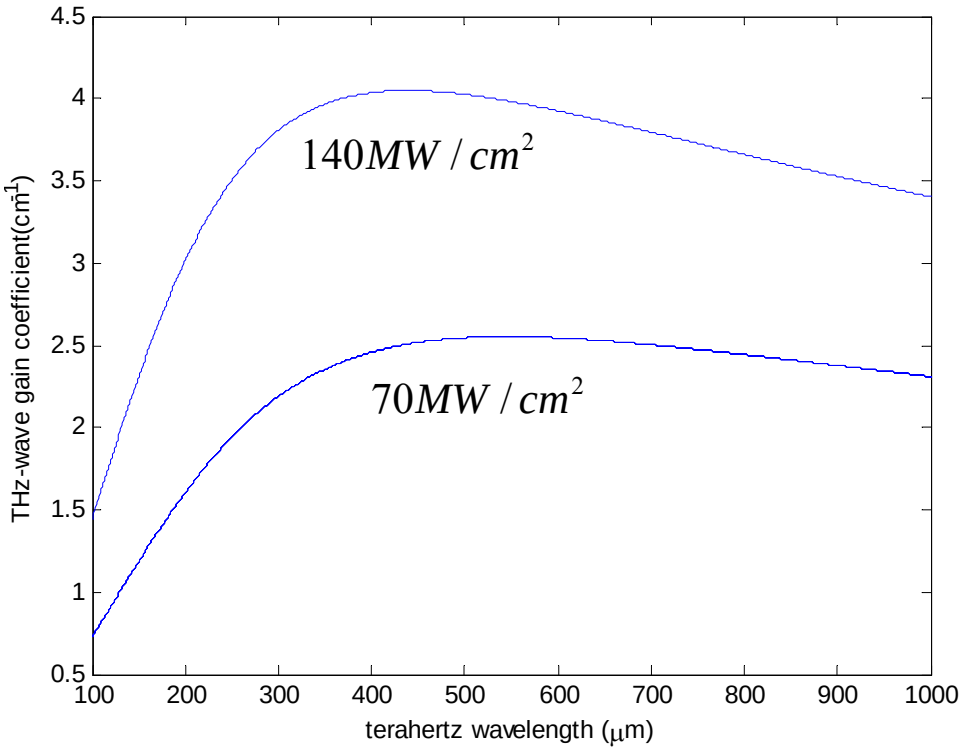


**Fig. 1-4** Calculated gain coefficients for parametric THz-wave generation in $LiNbO_3$ with 70 and 140 MW/cm$^2$ at 1064 nm.

***THz-wave parametric oscillator with an intra-cavity grazing-incidence grating***

In the past 10 to 15 years, the $LiNbO_3$-based TPO has been particularly exploited by Ito and Dunn Groups [17, 18]. However, in our group, we use two advanced improvements to increase the conversion efficiency and to narrow down the THz-wave linewidth.

One of the improvements utilizes the waveguide effect in the THz region. It can provide the low threshold and high conversion efficiency. Due to the helpful improvement, the thinner $LiNbO_3$ (1 mm thick) can be used as the TPO gain medium

[19, 20].

The other improvement utilizes the intra-cavity grazing-incidence grating configuration to reduce signal-wave linewidth. The intra-cavity grazing-incidence grating configuration has been applied in the single frequency, tunable lasers [21, 22, 23].

Because the THz-wave linewidth is the sum of the pump- and signal-wave linewidths, the pump laser is an injection-seeded actively Q-switched Nd:YAG laser with a 310-MHz linewidth at 1064nm. The seed laser to the pump is a homemade, single-longitudinal-mode, continuous-wave, diode-pumped Nd:$YVO_4$ laser with an intra-cavity Littman grating (1200 grooves/mm). Figure 1-5(a) shows the seed laser linewidth which is measured by Fabry-Perot scanning etalon. Using the angular dispersion of the grating, this seed laser can provide wavelength tunability (see Fig.1-6(b)). The wavelength tuning range can be tuned more than 0.42 nm. Finally, the narrow-line THz-wave radiation can be achieved.

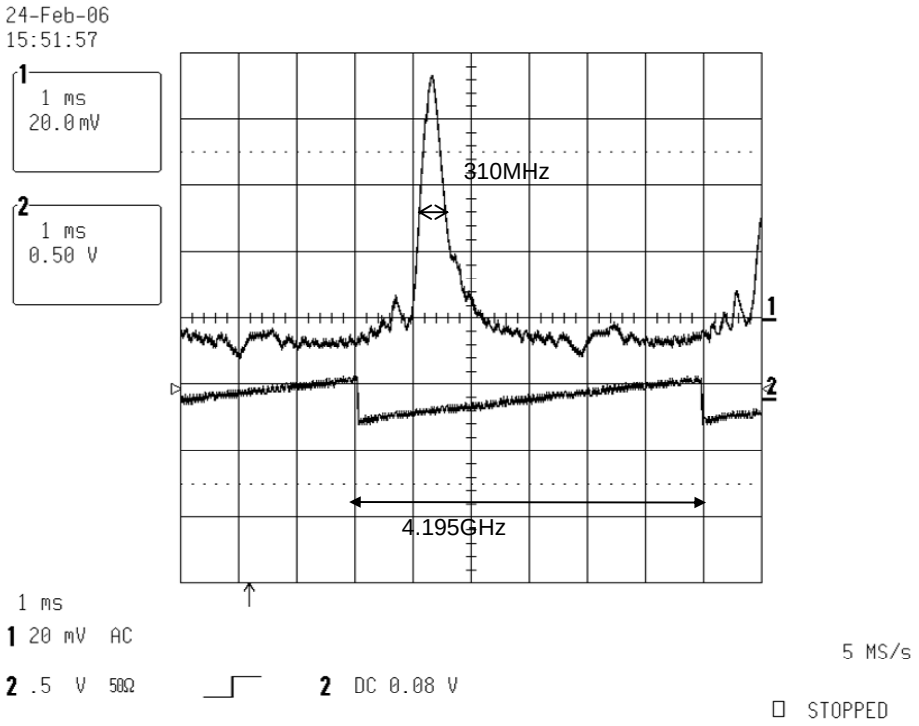


(a)

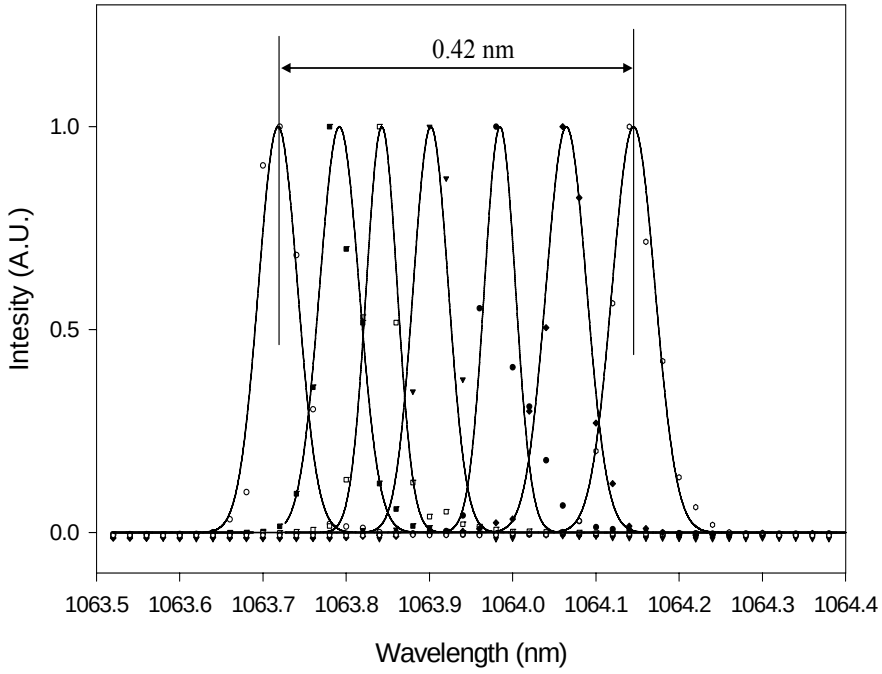


(b)

**Fig. 1-5** (a) The linewidth of the seed laser is measured by Fabry-Perot etalon scanning. (b) The tuning power spectra of the narrow-line 1064 nm laser radiation.

Figure 1-6(a) is the grazing incident TPO (GITPO) experimental setup. The phase-matching configuration is drawn at the upper-right corner of Fig. 1-6 (a) and the left side of Fig. 1-6(c). Based on two above-mentioned figures, the THz wave emits at ~65$^{o}$ from the signal beam direction and it is incident on the *y* surface at a ~26$^{o}$ angle. We attached a 240 μm-thick silicon-grating coupler (see Fig. 1-7) to the optically polished *y* surface of the $LiNbO_3$ crystal to avoid a total internal reflection and to extract the energy of the THz wave [24]. More details will be discussed in the chapter 3.

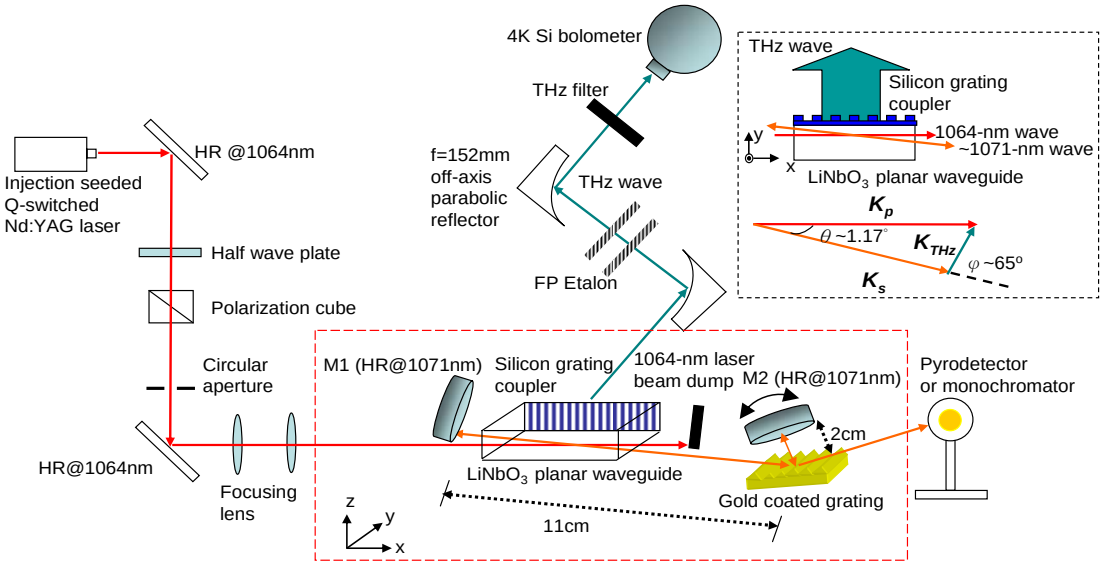


(a)

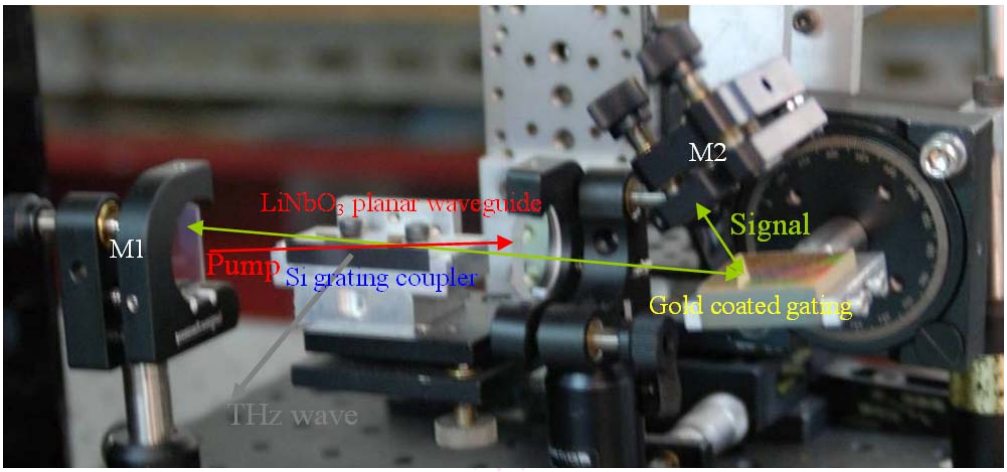


(b)

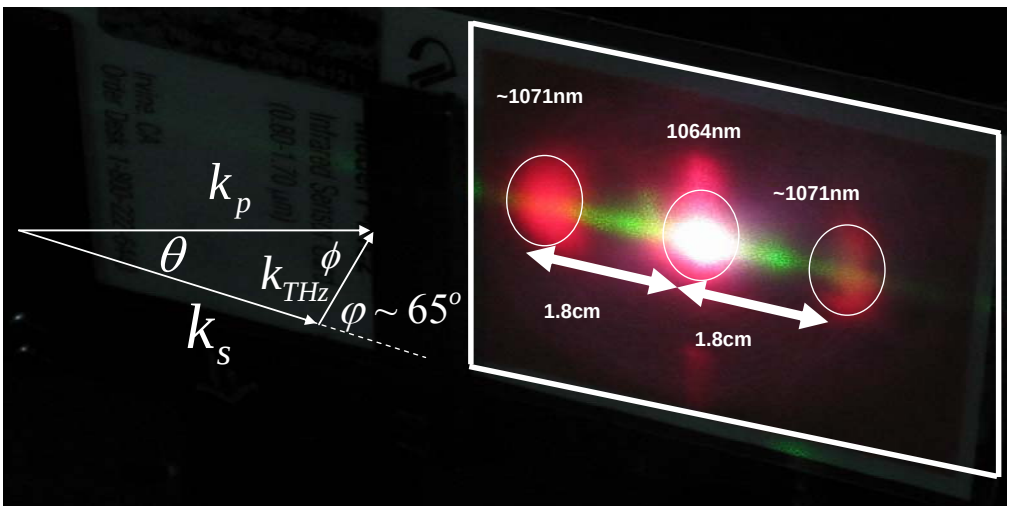


(c)

**Fig. 1-6** (a) The schematic of the GITPO pumped by an injection-seeded Q-switched Nd:YAG laser. It becomes a conventional TPO when the grating-M2 assembly is replaced

by an output coupler at the signal wavelength. Without the grating-M2 assembly, the setup can be used for studying a TPG. (HR: high reflection, FP: Fabry-Perot) (b) The photo for GITPO setup, GITPO cavity length is 13 cm. (c) Direct observation of the near-infrared signal wave of the terahertz-wave parametric generation with an IR card. Distance from the crystal end to the IR card is 40 cm and the separation between the pump and signal waves is 18 mm. The phase matching angle is approximately 1.17 degrees inside the crystal.

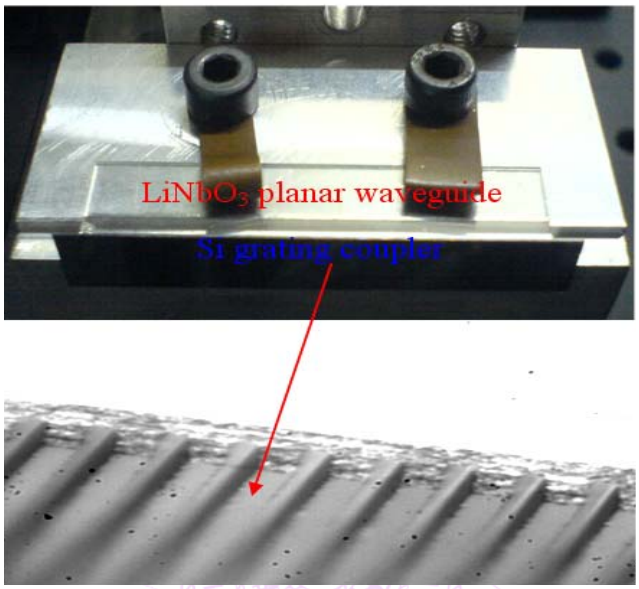


**Fig. 1-7** The THz-wave Si grating coupler with grating period and depth of is 125 and 50 μm, respectively. It is fabricated by a DISCO dicing saw.

## 1-5 Collinear Phased-matched Difference-frequency THz-wave Generation

### *Theory of forward and backward THz-wave difference-frequency generation*

The QPM technique [11] offers the advantage of the largest nonlinear coefficient in nonlinear optical materials and the feasibility of wavelength tunability. Among all the QPM crystals, PPLN has been widely applied in wavelength convertors [25] because of its larger nonlinear coefficient and wider transparent region. In addition, the thickness of the PPLN crystal usually falls in the 0.5 to 1 mm range, forming a one-dimensional waveguide at THz frequencies. The waveguide confinement for THz wave can greatly increase the THz-wave conversion efficiency. In this dissertation, we demonstrate forward and backward THz-wave difference-frequency generator (THz DFG) with an ultra-low pump power.

In MKS unit, the three couple wave equations for $E_{THz}$, $E_s$, and $E_p$ can be

expressed as

$$\begin{aligned}
\frac{dE_{THz}}{dz} &= \pm i\frac{\omega_{THz}\chi_P}{16\pi n_{THz}c_o}E_pE_s^*\exp\left(-i\Delta k_Q z\right)\mp\frac{1}{2}\alpha_{THz}E_{THz} \\
\frac{dE_s}{dz} &= i\frac{\omega_s\chi_P}{16\pi n_s c_o}E_pE_{THz}^*\exp\left(-i\Delta k_Q z\right)+i\frac{\omega_s\chi_R\left|E_p\right|^2}{8n_s c_o}E_s \\
\frac{dE_p}{dz} &= i\frac{\omega_p\chi_P}{16\pi n_p c_o}E_sE_{THz}\exp\left(i\Delta k_Q z\right)+i\frac{\omega_p\chi_R\left|E_s\right|^2}{8n_p c_o}E_p
\end{aligned} \tag{1-6}$$

where $n_{THz,\,s,\,p}$ denotes the refractive index for THz, signal, and pump wave in LiNbO3, respectively, and $\Delta k_Q = -\left(k_p - k_s \pm k_{THz} - \frac{2\pi}{\Lambda}\right)$ with a PPLN grating period $\Lambda$. (Notice: $+$ and $-$ represent forward and backward THz-wave direction, respectively.)

Due to the difference-frequency process, the pump depletion and the signal gain can be neglected. Therefore, the last two terms of Eq. 1-6 are dropped. Considering the boundary conditions for THz-wave forward and backward processes, $E_{THz}(0) = 0$ and $E_{THz}(L) = 0$ for the forward and backward process, respectively. The forward and backward THz-wave intensity can be expressed as [26]

$$I(L,0) = I_p I_s \frac{\pi^2}{4}\left(\frac{32d_{eff}^2 L^2\eta_o}{n_{THz}n_p n_s\lambda_s\lambda_{THz}}\right)\frac{\lambda_s}{\lambda_{THz}}\left[\frac{1-\exp\left(\pm i\Delta kL-\frac{\alpha_{THz}L}{2}\right)}{-\left(\pm i\Delta kL-\frac{\alpha_{THz}L}{2}\right)}\right]^2 \tag{1-7}$$

where $L$ is the crystal length; $\eta_o$ is the vacuum impedances; $I(L)$ and $I(0)$ are the forward and backward THz-wave intensity, respectively; $+$ and $-$ denote the forward and backward THz-wave direction, respectively.

If we take these three conditions (the crystal length is 3 cm, $I_p$ and $I_s$ are 85 MW/cm$^2$, and the PPLN grating period is 65 μm) into account, the normalized forward and backward intensity is shown in Fig. 1-8.

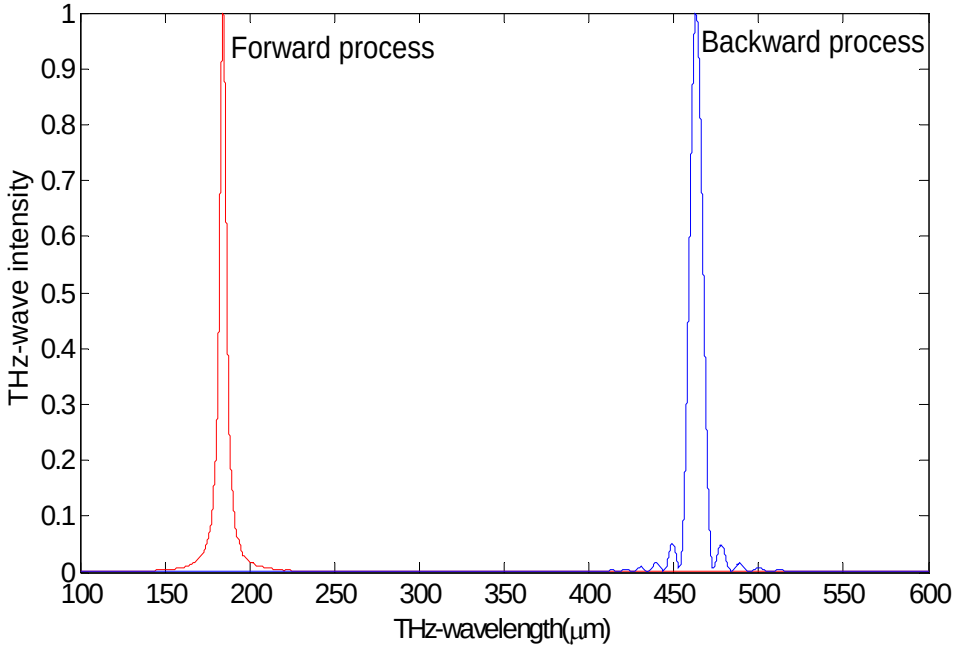


**Fig. 1-8** Normalized THz-wave intensity versus wavelength under the crystal length is 3 cm, $I_p$ and $I_s$ are 85 MW/cm$^2$, and the PPLN grating period is 65 μm.

There is a significant factor related to the tuning of the QPM parametric amplifier. The factor is

$$\Delta k_Q = k_p - k_s - k_i - k_m = 2\pi\left(\frac{n_p}{\lambda_p} - \frac{n_s}{\lambda_s} \pm \frac{n_{THz}}{\lambda_{THz}} - \frac{1}{\Lambda}\right). \tag{1-8}$$

The quasi-phase-matching is achieved when $\Delta k_Q = 0$. $k_m$ gives an additional parameter for tuning and is significantly powerful because it can be lithographically defined.

The wavelength tuning can be characterized by considering the quasi-phase-matching condition $\Delta k_Q = 0$. Therefore, the grating period can be determined from this condition and given by

$$\Lambda = \left[\frac{n(\lambda_p, T)}{\lambda_p} - \frac{n(\lambda_s, T)}{\lambda_s} - \frac{n(\lambda_{THz}, T)}{\lambda_{THz}}\right]^{-1}. \tag{1-9}$$

The energy conservation $\lambda_p^{-1} = \lambda_s^{-1} + \lambda_{THz}^{-1}$ should also be considered. The well-known Sellmeier equation determines the extraordinary refractive index of each

wavelength at a certain temperature. According to D. H. Jundt's measurement, the Sellmeier equation for $LiNbO_3$ during 0.4 to 3.4 μm wavelength region is [27]

$$n_e(\lambda,T)=\left[A_1+\frac{A_2+B_1\cdot F(T)}{\lambda^2-(A_3+B_2\cdot F(T))^2}+B_3\cdot F(T)-A_4\cdot\lambda^2\right]^{0.5}$$
$$[A_1,A_2,A_3,A_4]=[4.5820,0.09921,0.21090,0.021940]$$
$$[B_1,B_2,B_3]=[5.2716\times10^{-8},-4.9143\times10^{-8},22.971\times10^{-8}] \quad (1\text{-}10)$$
$$F(T)=(T-T_0)\times(T+T_0+546)$$
$$T_0=24.5^oC$$

The extraordinary refractive index at the THz-frequency region is expressed as [14]

$$n(\lambda_{THz})=\mathrm{Re}\left[\left(\varepsilon_\infty+\sum_j\frac{S_j\nu_{oj}^2}{\nu_{oj}^2-\nu^2-i\nu\Gamma_j}\right)^{\frac{1}{2}}\right] \quad (1\text{-}12)$$

where all the parameters in Eq. 1-12 are listed in Table 1-1.

Figure 1-9 shows the wavelength tuning curves for the 1538.98 nm pumped forward and backward THz-wave difference-frequency generation process. For such pump lasers, the QPM grating periods can be comfortably achieved through the recent PPLN fabrication technique.

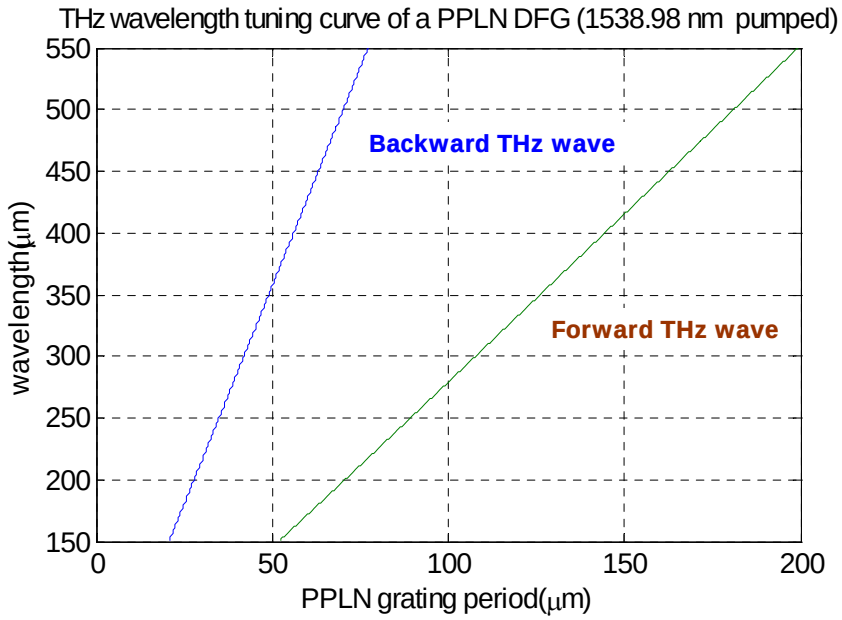


**Fig. 1-9** Wavelength tuning curves for 1538.98-nm pumped forward and backward THz-wave DFGs at room temperature. The horizontal axis is the first-order QPM grating period and the vertical axis is the phase-matched THz wavelength.

***Forward and backward THz-wave difference-frequency generation from periodically poled lithium niobate (PPLN)***

The difference-frequency generation is the convenient method for producing coherent THz-wave radiation. This type of generation has been demonstrated in THz-wave surface emitting in PPLN [28]. As the interaction length between the pump source and the THz wave is limited, the THz-wave generation efficiency is quite low. In contrast, collinear process provides a longer crystal length.

First, we fabricated a PPLN crystal with a grating period of 63 μm to 70 μm in 1 mm increments. According to THz wavelength curve (Fig. 1-9), we can predict that the 200 μm forward THz wave and the 500 μm backward can be generated in a 63 μm -70 μm PPLN crystal. Second, we constructed a dual-wavelength optical parametric amplifier (OPA) system as the THz-wave difference-frequency pump source. Figure 1-10 shows the THz-wave DFG dual-wavelength pump source starts from the distributed-feedback diode laser (DFBDL) and external-cavity diode laser (ECDL). These two diode lasers would then be amplified by the Erbium-doped fiber amplifier (EDFA) and OPA system. Figure 1-11 shows the photos of the forward and backward THz-wave generation.

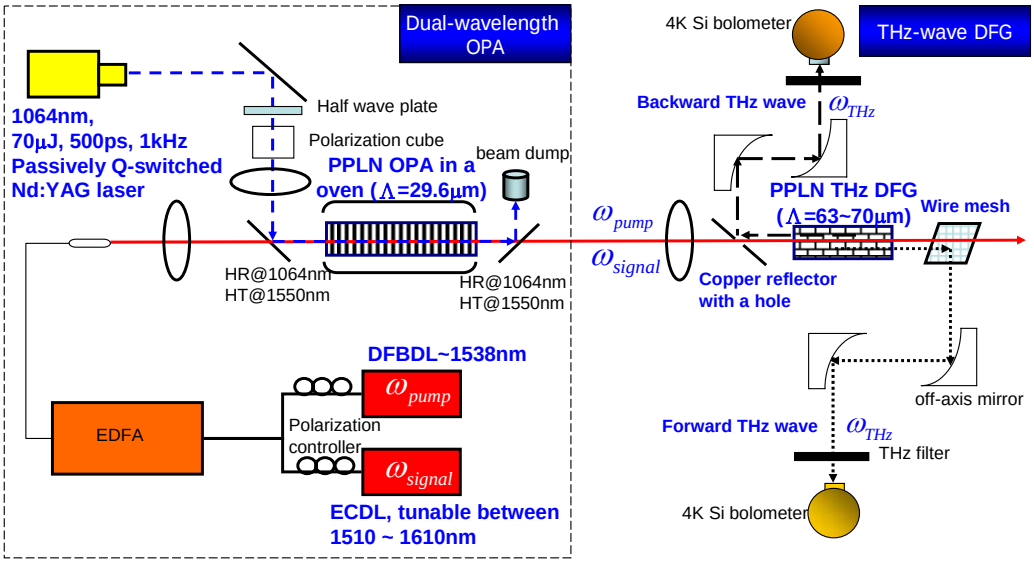


**Fig. 1-10** Setup of the collinearly quasi-phase-matched forward and backward THz difference frequency generations in a multi-grating PPLN crystal. (HR: high reflection, HT: high transmission, OPA: optical parametric amplifier, DFG: difference frequency generator, FP: Fabry-Perot spectrometer, ECDL: external-cavity diode laser, DFBDL: distributed-feedback diode laser, EDFA: Erbium-doped fiber amplifier.)

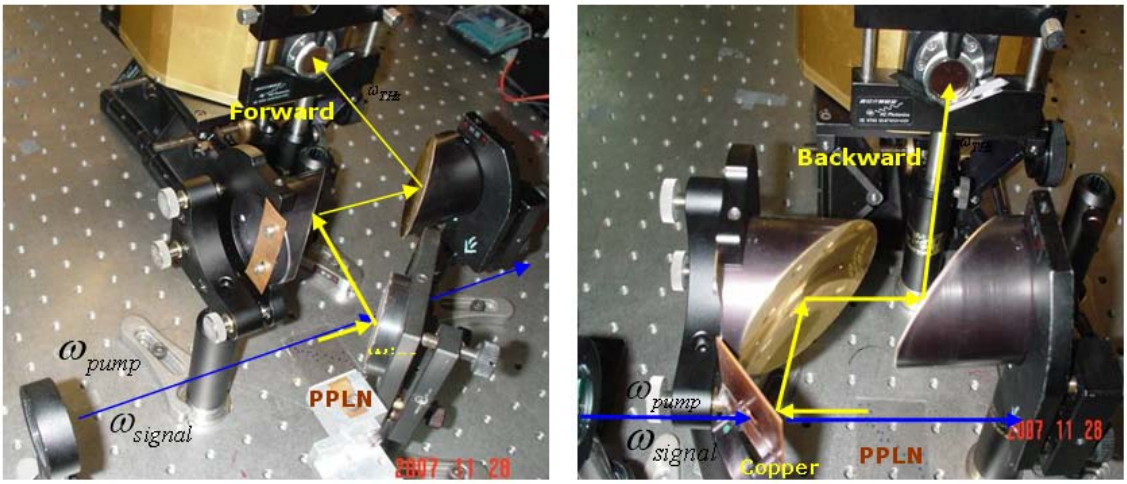


**Fig. 1-11** Photographs of forward and backward THz-wave generator.

## 1-6 Overview of this Dissertation

The accomplishments of the work presented in the dissertation are the parametric generation of THz-wave in non-collinear configuration and the QPM laser devices that produce THz-wave difference-frequency generations in collinear configuration. Regardless of the non-collinear or collinear configuration, our goal is to achieve a tunable, low-pump-power coherent THz source.

The organization of this dissertation is as followings: Chapter1 introduces the basic concept of the THz-wave generation. Chapter 2 gives the enhanced THz-wave parametric generation and oscillation in $LiNbO_3$ waveguides at THz frequencies. Chapter 3 establishes the ultra-low-threshold, narrow-line THz-wave parametric oscillator with an intra-cavity grazing-incidence grating. Chapter 4 discusses the forward and backward THz-wave difference-frequency generations from PPLN. Finally, Chapter 5 concludes the dissertation by presenting its contributions and future directions.

## References


1 C. Rønne, P. Åstrand, and S. R. Keiding, "THz spectroscopy of liquid $H_2O$ and $D_2O$," Phys. Rev. Lett. **82**, 2888-2891 (1999).

2 E. Knoesel, M. Bonn, J. Shan, and T. F. Heinz, "Charge transport and carrier dynamics in liquids probed by THz time-domain spectroscopy," Phys. Rev. Lett. **86**, 340-343 (2001).

3 K. Kawase, Y. Ogawa, Y. Watanabe, and H. Inoue, "Non-destructive terahertz imaging of illicit drugs using spectral fringeprints," Opt. Express. **11**, 2549-2554 (2003).

4 Q. Wu, T. D. Hewitt, and X.-C. Zhang, "Two-dimensional electro-optic imaging of THz beams," Appl. Phys. Lett. **69**, 1026-1028 (1996).

5 5. P. R. Smith, D. H. Auston, and M. C. Nuss, "Subpicosecond photoconducting dipole antennas," IEEE J. Quantum Electron. **24**, 255-256 (1988).

6 X.-C., B. B. Hu, J. T. Darrow, and D. H. Auston, "Generation of femtosecond electromagnetic pulses from semiconductor surface," Appl. Phys. Lett. **56,** 1011-1013 (1990).

7 D. H. Levy, *Free Electron Lasers and Other Advanced Sources of Light*, National Academy Press Washington, DC, 24–31(1994).

8 M. A. Piestrup, R. N. Fleming, and R. H. Pantell, "Continuously tunable submillimeter Wave Source," Appl. Phys. Lett**. 26**, 418-419(1975).

9 K. Kawase, M. Sato, T. Taniuchi, and H. Ito, "Coherent tunable THz wave generation from $LiNbO_3$ with monolithic grating coupler," Appl. Phys. Lett. **68**, 2483-2485 (1996).

10 K. Kawase, J. Shikata, and H. Ito, "Terahertz wave parametric source," J. Phys. D: Appl. Phys. **35**, R1-R14 (2002).

11 J. A. Armstrong, N. Bloemergen, J. Ducuing, and P. S. Pershan, "Interactions between light waves in a nonlinear dielectric," Phys. Rev., **127**, 1918-1939 (1962).

12 S. E. Harris, "Proposed backward wave oscillation in the infrared," Appl. Phys. Lett. **9**, 114-115 (1966).

13 C. Canalias, and V. Pasiskevicius, "Mirror-less optical parametric oscillator," Nature Photonics **1**, 459-462 (2007).

14 S. S. Sussman, "Tunable light scattering from transverse optical modes in lithium niobate," Microwave Lab. Report No. 1851, (Stanford University, Stanford, Calif., 1970).

15 Robert W. Boyd, *Nonlinear Optics*, 2nd ed. (Academic Press, INC., London, 2003), p.48.

16 M. Born and K. Huang, *Dynamic Theory of Crystal Lattice*, Clarendon Press, Oxford, 1954.

17 K. Kawase, J. Shikata, and H. Ito, "Terahertz wave parametric source," J. Phys. D: Appl. Phys. **35**, R1-R14 (2002).

18 T. J. Edward, D. Walsh, M. B. Spurr, C. F. Rae, M. H. Dunn, and P. G. Browne, "Compact source of continuously and widely tunable terahertz radiation," Opt. Express **14**, 1582-1589 (2006).

19 A. C. Chiang, T. D. Wang, Y. Y. Lin, S. T. Lin, H. H. Lee, Y. C. Huang, and Y. H. Chen, "Enhanced terahertz-wave parametric generation and oscillation in lithium niobate waveguides at terahertz frequencies," Opt. Lett. **30**, 3392-3394 (2005).

20 T. D. Wang, Y. Y. Lin, S. Y. Chen, A. C. Chiang, S. T. Lin, and Y. C. Huang, "Low-threshold, narrow-line THz-wave parametric oscillator with an intra-cavity grazing-incidence grating," Opt. Express **16**, 12571-12576 (2008)

21 K. C. Harvey and C. J. Matt, "External-cavity diode laser using a grazing-incidence diffraction grating," Opt. Lett. **16**, 910-912 (1991).

22 Y. Y. Lin, S. Y. Chen, A. C. Chiang, R. Y. Tu, Y. C. Huang, Y. F. Chen, and Y. H. Chen, "Single-longitudinal-mode, tunable dual wavelength, CW Nd:YVO4 laser," Opt. Express **14**, 5329-5334 (2006).

23 C. S. Yu and A. H. Kung, "Grazing-incidence periodically poled $LiNbO_3$ optical parametric oscillator," J. Opt. Soc. Am. B **16**, 2233-2238 (1999).

24 K. Kawase, M. Sato, T. Taniuchi, and H. Ito, "Coherent tunable THz wave generation from $LiNbO_3$ with monolithic grating coupler," Appl. Phys. Lett. **68**, 2483-2485 (1996).

25 A. C. Chiang, T. D. Wang, Y. Y. Lin, C. W. Lau, Y. H. Chen, B. C. Wong, Y. C. Huang, J. T. Shy, Y. F. Chen, and P. H. Tsao, "Pulsed optical parametric generation, amplification, and oscillation in periodically poled lithium niobate crystal," IEEE J. Quantum Electron. **40**, 791-799 (2004)

26 Y. J. Ding, J. B. Khurgin, "A new scheme for efficient generation of coherent and incoherent submillimeter to THz waves in periodically-poled lithium niobate," Opt. Commun. **148**, 105-109 (1998).

27 D. H. Jundt, "Temperature-dependent Sellmeier equation for index of refraction, $n_e$, in congruent lithium niobate," Opt. Lett. **22**, 1553-1555 (1999).

28 Y. Sasaki, A. Yuri, K. Kawase, and H. Ito, "Terahertz-wave surface-emitted difference frequency generation in slant-stripe-type periodically poled LiNbO3 crystal," Appl. Phys. Lett. **81**, 3323-3325 (2002).

# Chapter 2 Enhanced Terahertz-wave Parametric Generation and Oscillation in Lithium Niobate Waveguides at Terahertz Frequencies

In chapter 2, we observed parametric-generation efficiency of 1.61% from 1064 nm to 1071 nm and 162 μm in a 0.5-mm-thick, 45-mm-long z-cut congruent lithium-niobate waveguide with a pump energy of 2.2 mJ and a pump pulse width of 5.8 ns. We also measured an ultra-low threshold intensity of 70 MW/cm$^2$ for a 1064-nm pumped parametric oscillator resonating at 1071 nm and emitting at 162 μm using a 1-mm-thick, 45-mm-long lithium niobate waveguide.

## 2-1 Introduction

There are a number of ways for generating coherent terahertz (THz) radiations. For example, a free electron laser is useful for generating widely tunable and high-power THz radiations [1]. However, the relatively large size and high cost of a free electron laser have restricted its usage inside a national-scale laboratory. An emerging compact coherent THz source employs quantum cascade lasers under cryogenic cooling [2]. At room temperature THz-wave polariton scattering from lithium niobate ($LiNbO_3$) crystals pioneered by Pantell [3] has been greatly improved by Ito's group [4] in the past decade. Since a $LiNbO_3$ crystal has a transverse optical phonon mode that is Raman-active and infrared absorptive, the THz parametric gain in $LiNbO_3$ mostly originates from the cooperative coupling between the electronic and ionic nonlinearity. To date, all the THz nonlinear frequency mixing processes done in $LiNbO_3$ adopted a non-collinear phase-matching configuration in bulk crystals, in which a near infrared pump laser is polarized along the crystallographic z direction and a THz radiation is generated at a ~65$^o$ angle from the pump laser [5]. Waveguide confinement of mixing waves is known to enhance the efficiency in a nonlinear frequency mixing process. By taking the advantage of THz mode confinement in a $LiNbO_3$ slab waveguide, we report in this chapter efficient THz-wave parametric generator (TPG) and oscillator (TPO) with relatively low pump intensity at 1064 nm.

## 2-2 Experimental Configuration of the THz-wave Parametric Generation and Oscillation in Waveguides at Terahertz Frequencies

For what follows we call the short-wavelength output photon of the optical parametric process as the signal output [6], and the far-infrared output photon as the THz-wave output. Figure 1 shows the schematic of our TPG and TPO experiments. The pump source is an actively Q-switched Nd:YAG laser, producing laser pulses at 1064 nm with a 5.8-ns pulse width. The pump laser was first attenuated by a polarizer following a half-wave plate and focused into a $LiNbO_3$ nonlinear waveguide. The two off-axis flat reflectors having 99.5% reflectance at 1071 nm form a singly resonant THz-wave parametric oscillator. Without the two reflectors, the 1064-nm pumped $LiNbO_3$ waveguide is a THz parametric generator. The nonlinear waveguides used in the experiments were three 45-mm long, 15-mm wide double-side polished z-cut congruent $LiNbO_3$ slabs with thicknesses of 0.5, 0.78, and 1 mm. All three $LiNbO_3$ slabs were used in our TPG experiment for studying thickness dependence of waveguide-enhanced parametric gain. The 1-mm crystal slab was used for demonstrating high-efficiency, low-threshold TPO. Each crystal slab has a 65°-angle cut with respect to the pump beam for coupling out THz waves, as shown in Fig. 1. The input and output faces of the $LiNbO_3$ wafers were coated with anti-reflection dielectric layers at the signal and pump wavelengths. In this non-collinear phase-matched parametric process, all three mixing waves are polarized in the *z* or the waveguide-gap direction to utilize the largest nonlinear coefficient $d_{33}$ in $LiNbO_3$. Therefore the THz waves propagate in the $LiNbO_3$ waveguide are the transverse-magnetic (TM) wave.

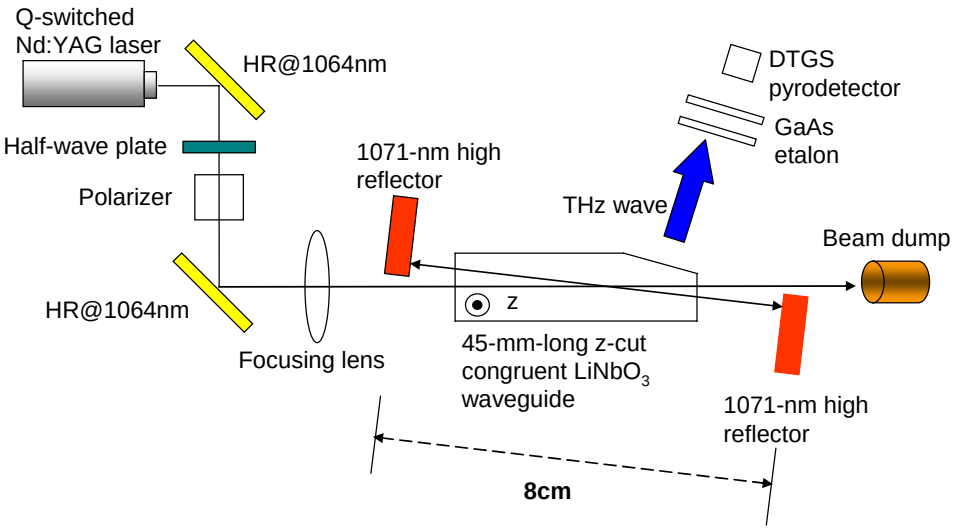


(a)

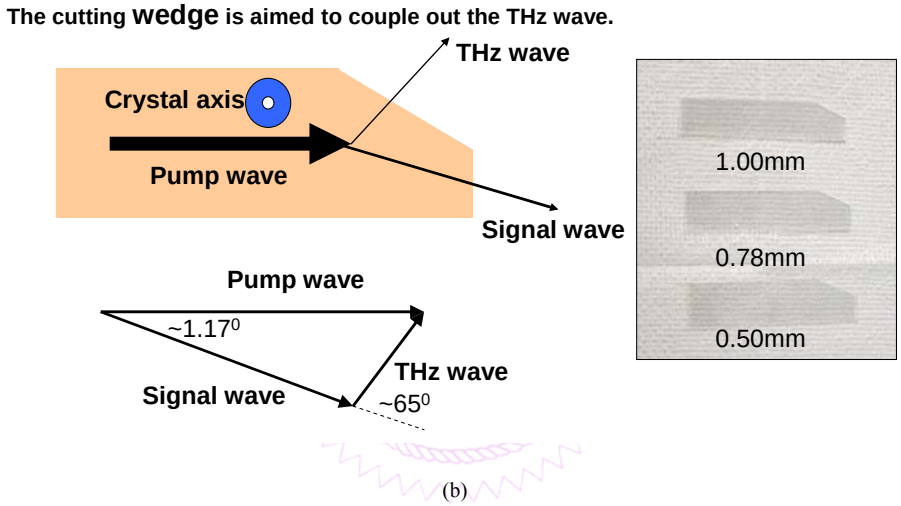


(b)

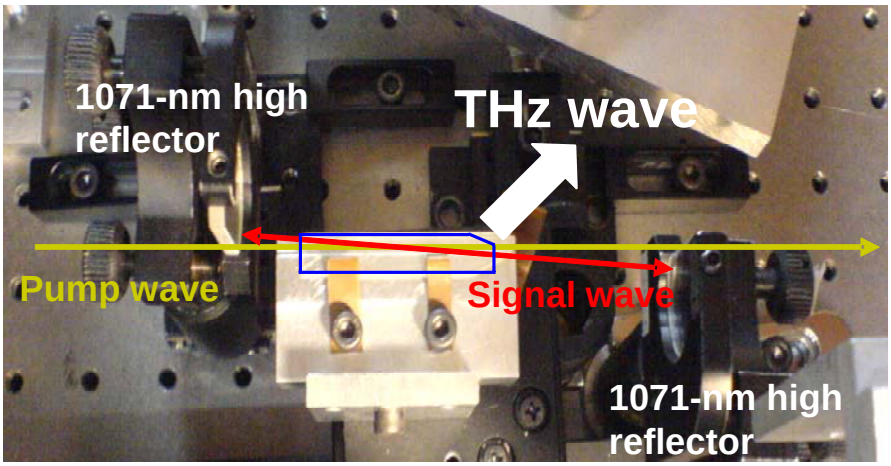


(c)

**Fig. 2-1** (a) Schematic of the waveguide TPO and TPG experiments. The TPO and TPG experiments were performed with and without the 1071-nm high reflectors, respectively. (b) Non-collinear phase-matched diagram and $LiNbO_3$ THz waveguide with 0.5-, 0.78-, and 1-mm thickness. (c) The Photograph of TPO experiment.

In a slab waveguide of thickness $t$ and refractive index $n_{THz}$ at the THz wavelength $\lambda_{THz}$, the maximum number of THz modes supported by the waveguide is given by [7] $m_{\max} = 2t\sqrt{n_{THz}^2 - 1}/\lambda_{THz}$. For example, the maximum numbers of the waveguide modes in 0.5-, 0.78-, and 1-mm-thick $LiNbO_3$ slab waveguides are 34, 52, and 67, respectively, assuming a refractive index of 5.4 at 160 μm. The confinement of THz waves in such highly multimode waveguides is still apparent, because the half diffraction angle of a THz wave at 160 μm is as large as 100 mrad for a beam diameter of 300 μm. Although there could be concerns on the generation of multiple THz-wave modes from parametric mixing in a sub-millimeter $LiNbO_3$ waveguide, it is clear that not all the waveguide modes can be excited but only those phase-matched modes with mode-field distributions well overlapped with the pump field can grow to some appreciable energy. If a $TEM_{00}$ pump field is aligned to the waveguide-gap center, an odd TM mode at THz having a transverse electric field anti-symmetric to the center of the waveguide gap is less likely to grow up. Since the lowest-order $TM_0$ mode has the largest overlapping integral with a center-aligned $TEM_{00}$ pump beam, it is therefore reasonable to assume that most THz output energy is still from the fundamental TM mode in the multimode nonlinear waveguides.

## 2-3 Experimental Results and Discussions

***Waveguide-enhanced Terahertz parametric generation***

Initially, we investigated the waveguide-enhanced TPG with different waveguide thicknesses. The waveguide effect is more significant when the pump beam is well overlapped with the THz waveguide mode. In the experiment, we passed a collimated pump beam through a 480-μm-diameter aperture and transmitted 2.2 mJ/pulse pump energy into each $LiNbO_3$ slab waveguide. In Table 2-1, we show the measured output characteristics of the signal wave from 0.5-, 0.78-, and 1-mm-thick waveguides under the same pumping condition. It is evident from Table 1 that the pump-to-signal energy conversion efficiency was increased by more than a factor of two when the thickness of the $LiNbO_3$ waveguide was reduced from 1 to 0.5 mm. The 1.61% single-pass

parametric efficiency and the generated signal energy from the 0.5-mm-thick waveguide have been greatly improved from previously reported values[4] for a 1064-nm pumped $LiNbO_3$ THz-wave parametric generator at 2.2-mJ pump energy. When the waveguide thickness was reduced from 1 to 0.5 mm, the signal pulse width was also reduced from 4 to 2.8 ns. The reduction in the signal pulse width is a signature of high-gain parametric generation in the thinner waveguide due to a highly nonlinear growth rate of the signal wave in an exponential-gain process. The higher parametric gain and THz-mode excitation also caused signal spectral broadening to the signal in thinner $LiNbO_3$ waveguides.

**Table 2-1.** TPG signal-wave output characteristics from 0.5-, 0.78-, and 1-mm-thick, 45-mm-long z-cut $LiNbO_3$ slab waveguides.

| $LiNbO_3$ waveguide thickness | Signal pulse width | Signal pulse energy | Conversion efficiency | Signal spectral width (FWHM) |
|---|---|---|---|---|
| 0.5 mm | 2.8 ns | 32.8 μJ | 1.61 % | 1 nm |
| 0.78 mm | 3.2 ns | 26.6 μJ | 1.31 % | 0.85 nm |
| 1 mm | 4.0 ns | 15.0 μJ | 0.75 % | 0.7 nm |

In order to investigate the THz-mode frequencies in the TPG process, we translated the 1-mm-thick $LiNbO_3$ waveguide in the z direction so that the pump laser was displaced vertically from the waveguide-gap center. At different vertical positions, the pump laser can selectively excite one or several high-order THz-wave modes with which the pump laser mode has a good overlap. The slightly different frequencies of the generated THz modes are encoded into the signal output spectrum according to the frequency-conservation law. Figure 2-2 shows that the measured center wavelength of the signal output spectrum indeed varies with the pump displacement from the waveguide-gap center $\Delta z$, where a positive $\Delta z$ denotes a pump beam above the waveguide-gap center. As expected, the signal-wavelength shift is symmetric about $\Delta z = 0$ due to the symmetry of the THz mode-field profile about the waveguide axis. The ~23 GHz signal-frequency shift for a pump displacement of $\Delta z = \pm 120$ μm is equal to the frequency spacing between the $TM_0$ and $TM_9$ THz-wave modes. We evaluated the overlapping integrals between the pump field and the TM mode fields and found a 15-GHz frequency shift in the signal's power spectrum for a

120-μm pump displacement from the waveguide axis. The difference of a few GHz between the calculated and the measured frequency shifts could be attributable to the ~±8 GHz uncertainty in the measurement and a numerical model not considering gain and loss of individual waveguide modes.

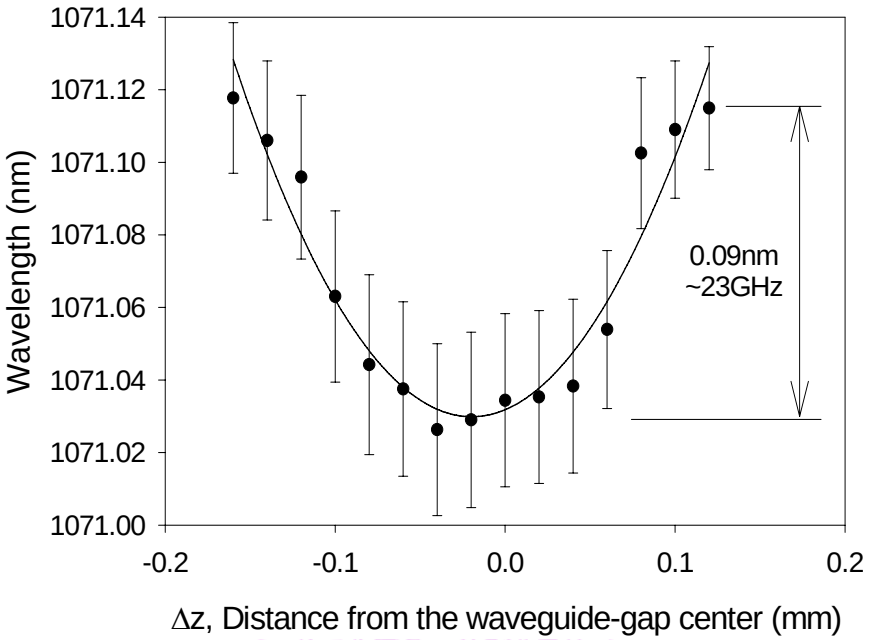


**Fig. 2-2** Signal wavelength versus the pump-beam position relative to the waveguide-gap center in the TPG experiment. A positive $\Delta z$ denotes the vertical displacement of the pump beam above the gap center. The 23-GHz frequency shift shown in the plot corresponds to the frequency spacing between the $TM_0$ and $TM_9$ modes of the THz waves in the waveguide.

***Waveguide-enhanced terahertz parametric oscillation***

We continued to perform THz parametric oscillation by using two off-axis flat mirrors to oscillate the 1071-nm signal wavelength in the 1-mm-thick, 45-mm-long $LiNbO_3$ waveguide. The two mirrors were separated by an 8-cm distance, permitting ~7 roundtrips for the signal wave in the cavity. The 1-mm-thick waveguide was chosen for a larger pump aperture and for ease of alignment. However the overlap between the pump mode and the THz-wave fundamental mode was improved by transmitting a 3.6-mm-diameter, well collimated $TEM_{00}$ pump beam through a 0.8-mm-diameter circular aperture immediately before the front mirror of the parametric oscillator. Figure 2-3 shows the measured intra-cavity signal energy versus

the pump energy of the waveguide THz-wave parametric generator. It is seen that the oscillation threshold is apparently below 2 mJ in pump energy or 70 MW/cm$^2$ in pump intensity, which is, to the best of our knowledge, the lowest pump threshold ever reported for a $LiNbO_3$ THz-wave parametric oscillator [4]. An intracavity signal energy of 0.31 mJ was generated at a pump energy of 4.3 mJ or at a pump level 2.15 times above the threshold.

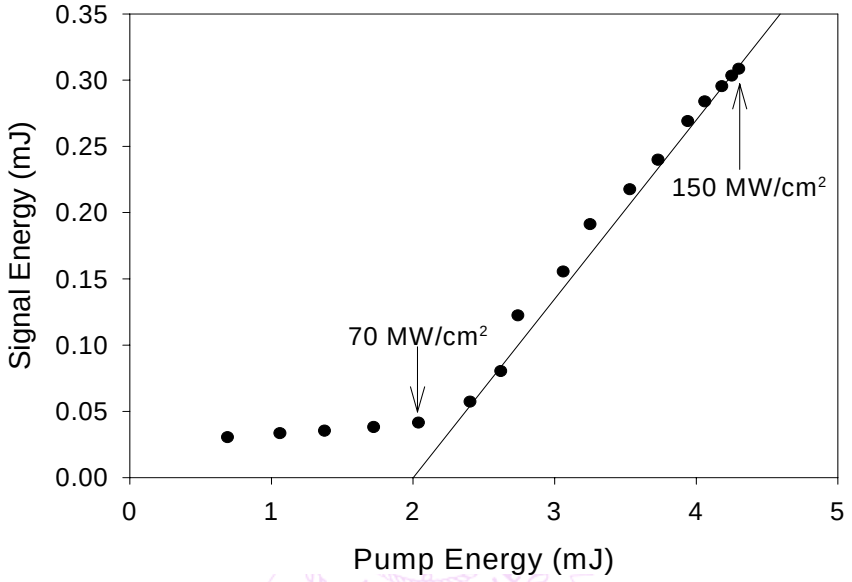


**Fig. 2-3** Intra-cavity signal energy versus pump energy of the waveguide THz parametric oscillator using a 1-mm-thick, 45-mm-long $LiNbO_3$ slab waveguide. The pump threshold at 1064 nm is as low as 70 MW/cm$^2$.

To measure the THz output wavelength, we used a room-temperature, deuterated triglycine sulfate (DTGS) pyrodetector immediately after an air-gap GaAs scanning etalon near the exit cut of the $LiNbO_3$ waveguide. Each of the two GaAs plates has a thickness of 0.633 mm. Figure 2-4 shows the fitting between the measured THz transmission and the Airy function. The characteristic period of the etalon transmission curve clearly indicates a THz wavelength of 162 μm. In the measurement, we averaged 1000 pulses for each data point and the signal-to-noise ratio at the peak transmission was about 7~10. Because we did not calibrate the DTGS detector, we were not able to deduce the exact output energy of the THz wave. In this work, the energy extraction technique for the THz wave was not optimized. It

is our next effort to maximize the energy extraction of the THz wave and calibrate the measured energy.

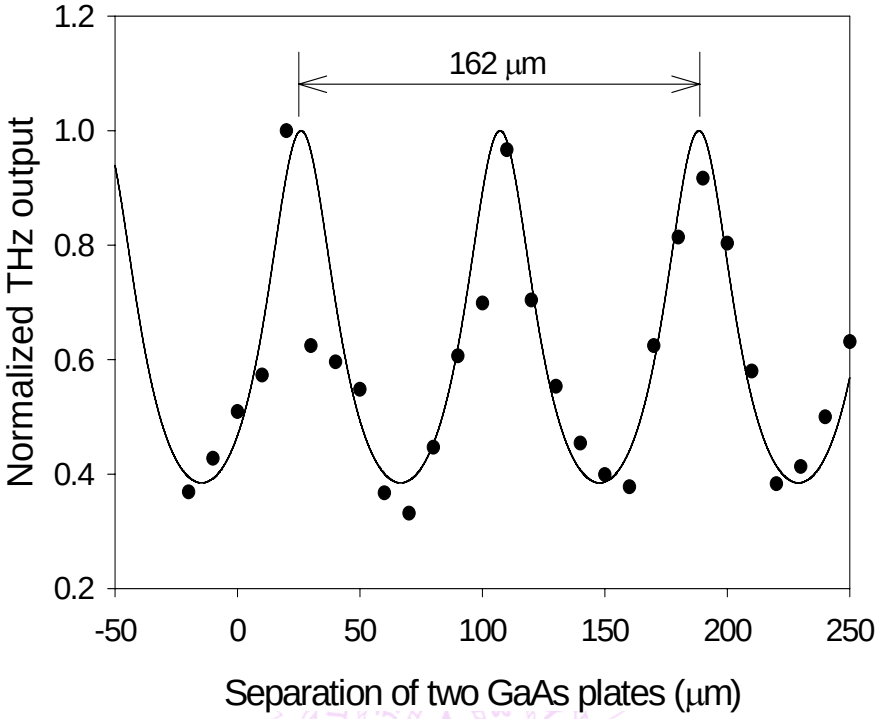


**Fig. 2-4** THz-wave intensity transmitted through a scanning GaAs etalon as a function of the etalon gap. A THz wavelength of 162 μm can be determined from the periodicity of the fitting curve.

## 2-4 Summary

In Summary, we have demonstrated high-gain, high-efficiency TPG and TPO in $LiNbO_3$ slab waveguides. Waveguide-enhanced parametric gain was confirmed from the two-time increase in parametric conversion when the $LiNbO_3$ thickness was reduced from 1 mm to 0.5 mm under the same pump condition. With 2.2-mJ pump energy at 1064 nm, a single-pass parametric conversion of 1.61% was achieved from a 0.5-mm-thick, 45-mm-long z-cut $LiNbO_3$ THz slab waveguide. Using a 1-mm-thick, 45-mm-long $LiNbO_3$ multi-mode waveguide at THz, we also demonstrated a waveguide parametric oscillator with an ultra-low threshold intensity of 70 MW/cm$^2$.

## References

1 W. B. Colson, "Short wavelength free electron lasers in 1998," Nucl. Inst. Meths **A429**, 37-40 (1999).

2 Qing Hu, "Terahertz quantum cascade lasers," Technical Digest, CTuM3, Conference on Lasers and Electro-optics, Baltimore, May 24-26, 2005.

3 M. A. Piestrup, R. N. Fleming, and R. H. Pantell, "Continuously tunable submillimeter wave source", Appl. Phys. Lett. **26**, 418-421 (1975).

4 K. Kawase, J. Shikata, and H. Ito, "Terahertz wave parametric source," J. Phys. D. **35**, R1-14 (2002).

5 Y. Sasaki, A. Yuri, K. Kawase, and H. Ito, "Terahertz-wave surface-emitted difference frequency generation in slant-stripe-type periodically poled $LiNbO_3$ crystal," Appl. Phys. Lett. **81**, 3323-3325 (2002).

6 M. Bass, J. M. Enoch, E. W. Van Stryland, W. L. Wolfe, *Handbook of Optics* **IV** (McGraw-Hill, 2001) 22.2.

7 B. E. A. Saleh and M. C. Teich, *Fundamentals of Photonics* (John Wiley & Sons, 1991) 251.

# Chapter 3 Low-threshold, Narrow-line Terahertz-wave Parametric Oscillator with an Intra-cavity Grazing-incidence Grating

In chapter 3, we report a low-threshold, narrow-line terahertz-wave parametric oscillator with an intra-cavity grazing-incidence grating and a 1-mm thick, 45-mm long lithium-niobate planar waveguide. When pumped by an actively Q-switched Nd:YAG laser, the threshold energy and intensity of the parametric oscillator were about 2.2 mJ and 70 MW/cm$^2$, respectively. The linewidths of the output THz wave were 12 and 134 GHz with and without the intra-cavity grating, respectively.

## 3-1 Introduction

To date, terahertz-wave radiations are mostly generated in the form of either broad-band electromagnetic pulses or narrow-band electromagnetic waves. The latter is a laser-like coherent radiation and is the focus of this paper. Among various methods for generating terahertz (THz) radiations, nonlinear frequency mixing is known to offer an effective means to obtain coherent THz-wave radiations at room temperature. In particular, in the past 10-15 years Ito *et al.* [1, 2, 3, 4, 5, 6] have demonstrated several promising THz-wave parametric amplifiers and oscillators using lithium niobate ($LiNbO_3$) as the parametric gain medium. The THz wave emits at about 64° from the pump direction of an optical wave in the $LiNbO_3$ crystal. The non-collinear phase-matching configuration and fast diffraction of the THz wave in the bulk $LiNbO_3$ crystal exacerbate the poor parametric efficiency due to strong absorption of the THz wave in $LiNbO_3$. Recently Edward *et al.* were able to lower the threshold energy of the $LiNbO_3$ THz-wave parametric oscillator (TPO) to about 1 mJ by installing a $LiNbO_3$ TPO in a pump-laser cavity [7]. A narrow linewidth is also often desirable for a coherent radiation source. Although a conventional TPO is known to start from the amplification of spontaneous noise, Imai *et al.* demonstrated a single-frequency pumped TPO with a 200-MHz output linewidth by using a MHz-linewidth seeding signal [1]. To the best of our knowledge, all the previously reported $LiNbO_3$ TPOs without signal seeding had an output linewidth larger than 20

GHz [5, 6]. The aim of our work is to demonstrate an externally pumped $LiNbO_3$ TPO starting from spontaneous noise while having both the lowest threshold [8] and the narrowest linewidth to date.

A THz waveguide is known to confine the THz radiation and enhance the parametric conversion efficiency of a TPO [9, 10]. It has also been demonstrated in the optical-frequency regime that an intra-cavity grazing-incidence grating can greatly narrow down the linewidth and offer wavelength tunability of a laser [11, 12, 13]. By taking advantage of the THz waveguide in our previous work [9] and the intra-cavity grazing-incidence grating, we demonstrate in this paper a low-threshold and narrow-line TPO in a $LiNbO_3$ planar waveguide.

## 3-2 Experimental Configuration of the THz-wave Parametric Oscillator with an Intra-cavity Grazing-incidence Grating

Figure 3-1 shows the schematic of the grazing-incidence TPO (GITPO) with an intra-cavity grating. The pump laser is an injection-seeded actively Q-switched Nd:YAG laser, producing 5.8-ns laser pulses at 1064 nm with a 310-MHz linewidth. The seed laser to the pump is a homemade, single-longitudinal-mode, continuous-wave, diode-pumped $Nd:YVO_4$ laser with an intra-cavity Littman grating. To improve the overlap between the pump and the THz waves in the $LiNbO_3$ crystal, we cut the Gaussian tail of the $TEM_{00}$ pump mode by transmitting a well collimated, 3.6-mm-diameter pump beam through a 0.8-mm-diameter aperture before the GITPO. After the aperture, the pump beam was focused to the center of a congruent $LiNbO_3$ crystal with dimensions of 45, 15, and 1 mm along the crystallographic *x*, *y*, and *z* directions. The 1-mm thick crystal can accommodate many THz-wave modes, but the $TM_0$ mode has the largest overlap integral with a well aligned pump mode and is the mode most likely to grow [9]. The *x* surfaces of the crystal were optically polished and an anti-reflection coated film at the pump (1064 nm) and signal (~1071 nm) wavelengths. The polarization of the pump laser was aligned along the *z* direction so that the highest nonlinear coefficient, $d_{33}$, can be used for parametric wave mixing. We constructed the GITPO by using two flat mirrors highly reflecting at the signal wavelength (M1 and M2, reflectance > 99.5% @~1071 nm) and an intra-cavity

gold-coated grating (Edmund Scientific NT55-263, 1200 grooves/mm, blaze angle = 36°52'). The resonant cavity of the GITPO, formed by mirrors M1 and M2, has a length of 13 cm. At the 85° grazing-incidence angle for a TM wave at the signal wavelength, the single-pass resolution of the intra-cavity grating is 24.5 GHz and the diffraction efficiency of the 1st-order beam is 57.5%. Since the signal wave reflects twice on the grating for the each round-trip propagation in the cavity, the effective resonator loss is about 67%. Fine tuning of the THz-radiation wavelength can be achieved by rotating the angle of mirror M2. In our experiment, we can remove the grating-M2 assembly to study the experiment for a THz-wave parametric generator (TPG.). When comparing the GITPO with a conventional TPO, we replaced the grating-M2 assembly with a flat mirror (50% transmittance @ 1071 nm) as the output coupler. The TPO in our comparison study has a cavity length the same as that of the GITPO.

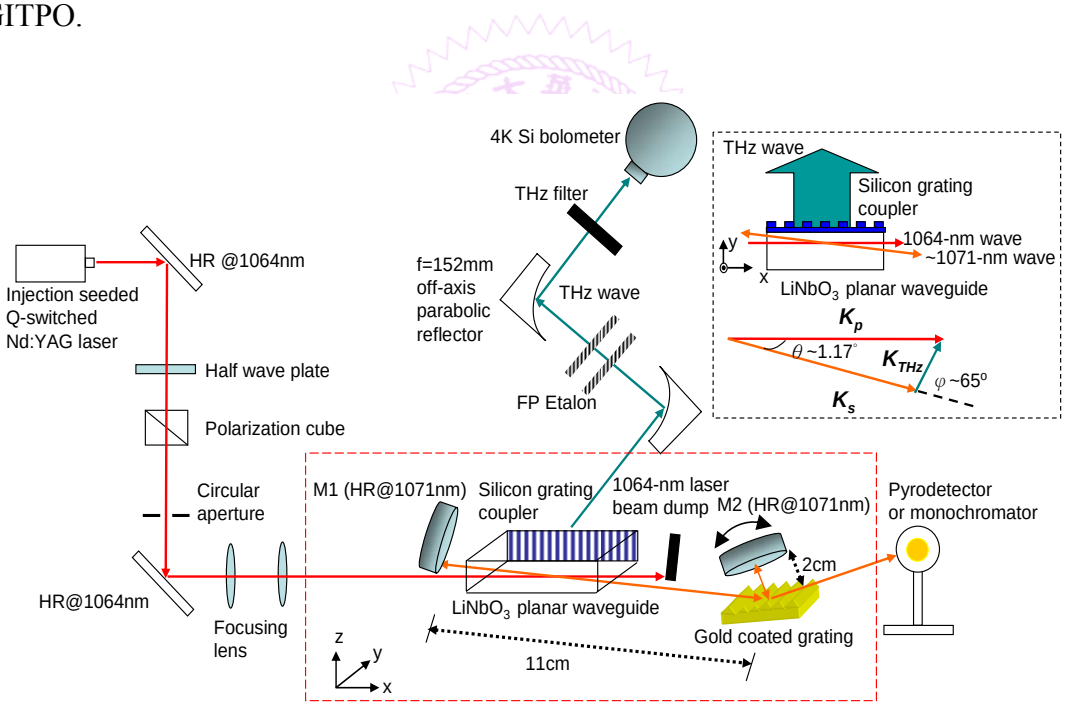


**Fig. 3-1** The schematic of the GITPO pumped by an injection-seeded Q-switched Nd:YAG laser. It becomes a conventional TPO when the grating-M2 assembly is replaced by an output coupled at the signal wavelength. Without the grating-M2 assembly, the setup can be used for studying a TPG. (HR: high reflection, FP: Fabry-Perot)

One of the *y* surfaces of the $LiNbO_3$ crystal is optically polished. As shown by the phase-matching configuration at the upper-right corner of Fig. 1, the THz wave

emits at ~65° from the signal beam direction and is incident on the *y* surface at a ~26° angle. We attached a 240-μm-thick silicon-grating coupler to the optically polished *y* surface to avoid total internal reflection and extract the energy of the THz wave [3]. The grating period, groove depth, and the groove width of the silicon grating are 125, 50, and 65 μm, respectively. The grating formula governs the relationship between the incidence and diffraction angles of the THz wave, given by $\sin\theta_m = n_{Si}\sin\theta_{si} - m\lambda/\Lambda$, where $\Lambda$ is the grating period, and $\theta_m$ is the $m^{\text{th}}$-order diffraction angle, $\theta_{si} = \sin^{-1}\left(n_T / n_{Si}\sin\theta_i\right)$ is the incident angle of the THz wave in the silicon grating with $\theta_i$~26° being the incident angle of the THz wave in the $LiNbO_3$, and $n_T$ (~5.25) and $n_{Si}$ (~3.4) are the refractive indices of the $LiNbO_3$ and the silicon wafers at THz frequencies, respectively. For the 164-μm THz wavelength in our experiment, the 1st-order and 2nd-order diffraction angles are nearly 90° and 18° from the surface normal of the grating.

Following the silicon-grating coupler, a set of off-axis parabolic mirrors (*f* = 152-mm, 2″-aperture) collects and collimates the THz-wave radiation into the 4K Si bolometer. The silicon grating is placed at the front focal plane of the first off-axis parabolic mirror. The spectrum of the infrared signal wave was measured by a typical 1/2-m grating monochromator (CVI DK480). We measured the THz wavelength by using a scanning Fabry-Perot (FP) etalon inserted between the two off-axis mirrors. The etalon was made from two parallel wire meshes containing 45 μm × 45 μm square apertures with a 54% filling factor. The transmittance of the wire mesh is 20% for an incident THz wave at 164 μm, yielding finesse of 14 for the scanning etalon spectrometer.

### 3-3 Experimental Results and Discussions

Figure 3-2 shows the output signal-wave energy versus pump energy of the TPG, TPO, and GITPO. The pump thresholds of the TPO and GITPO were found to be 1.9 mJ (60 MW/cm$^2$ pumping intensity) and 2.2 mJ (70 MW/cm$^2$ pumping intensity), respectively, which are, to the best of our knowledge [4, 6], the lowest oscillation thresholds ever reported for an externally pumped $LiNbO_3$ TPO [9]. At the maximum

pump energy 4.4-mJ (140MW/cm$^2$), the overall parametric conversion efficiencies of the TPG, TPO, and GITPO were 1.9%, 10.0%, and 5.0%, respectively. Since the round-trip optical loss at the grating is 67%, which is higher than the 50% output-coupling loss of the TPO, the pump threshold of the GITPO is slightly higher than that of the TPO. The low pump threshold and high efficiency were made possible from waveguide confinement of the THz wave and thus better spatial overlap between the pump and THz waves in the parametric gain region.

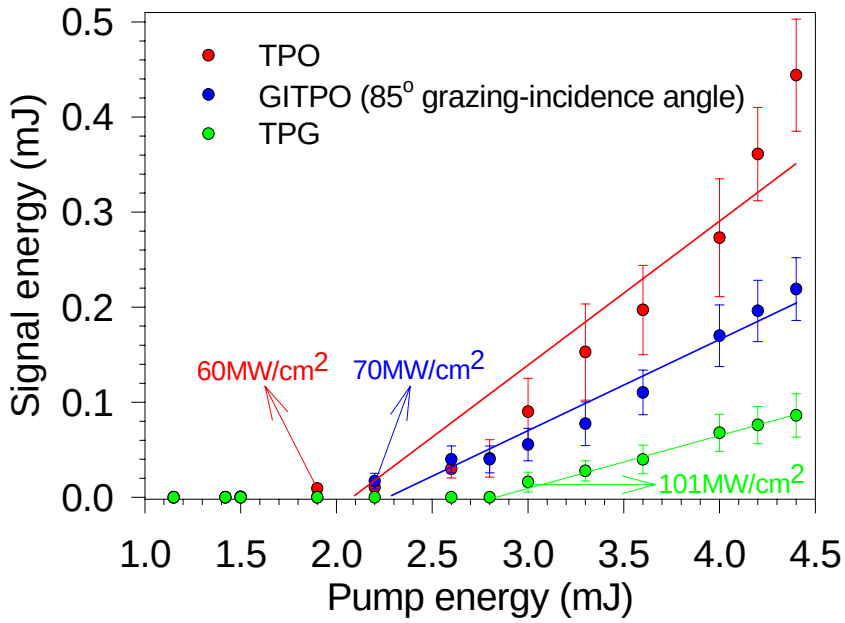


**Fig. 3-2** Signal versus pump energy of the TPG (green dots), TPO (red dots), and GITPO (blue dots) using a 1-mm-thick, 45-mm-long $LiNbO_3$ planar waveguide. The pump threshold intensities of the TPO and GITPO are shown in the plot.

Figures 3-3(a) and (b) show the temporal and spectral measurements for the signal wave, respectively, at 4.4-mJ pump energy. As expected, the signal-wave pulse width of the GITPO is slightly longer than that of the TPG in Fig. 3-3(a), because the parametric oscillation enhances the energy conversion in the trailing part of the signal pulse. In Fig. 3(b), the measured signal spectra of the TPG, TPO, and GITPO are 213, 134, and 12 GHz, respectively. It can be seen that the signal linewidth of the GITPO is greatly reduced from that of the TPG by ~18 times and TPO by ~11 times. Since the linewidth of the pump laser was measured to be 310 MHz, the THz-wave

linewidth can be inferred from the frequency relationship of parametric conversion

$$\omega_p = \omega_s + \omega_{THz} \tag{3-1}$$

with a known signal linewidth, where $\omega$ is the angular frequency of the mixing wave, and the subscripts *p*, *s*, and *THz*, denote the quantities associated with the pump, signal, and THz waves, respectively. From Equation 3-1, the linewidth of the THz wave is approximately 12 GHz. Given the specifications of the grating, it can be calculated that the single-pass grating bandwidth is 24.5 GHz at an $85^o$ grazing-incidence angle [13]. In theory, the signal and thus the THz-wave output linewidth of the GITPO is the single-pass grating bandwidth divided by the square root of the number of the round-trip propagations of the signal wave in the cavity [13]. With the 13-cm cavity length and 3.5-ns signal-wave pulse width, the number of the round-trip propagations is 4. Therefore the theoretical value of the THz-wave linewidth of the GITPO is 12.5 GHz, which is in good agreement with the value deduced from Fig. 3-3(b) and the frequency relationship (1). In Fig. 3-3(b), the spectrum of the signal wave or the frequency of the THz wave is tuned over a 130-GHz range by simply rotating the angle of mirror M2 by 0.6 mrad. In this GITPO, the grating-M2 assembly offers excellent spectral stability to the output THz wave, which is usually not available from a conventional TPO.

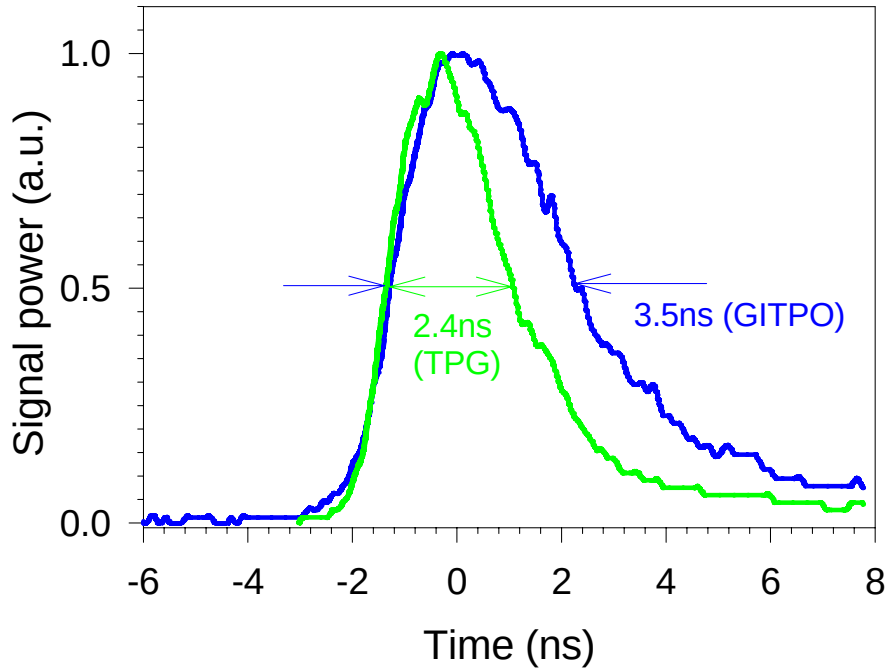


(a)

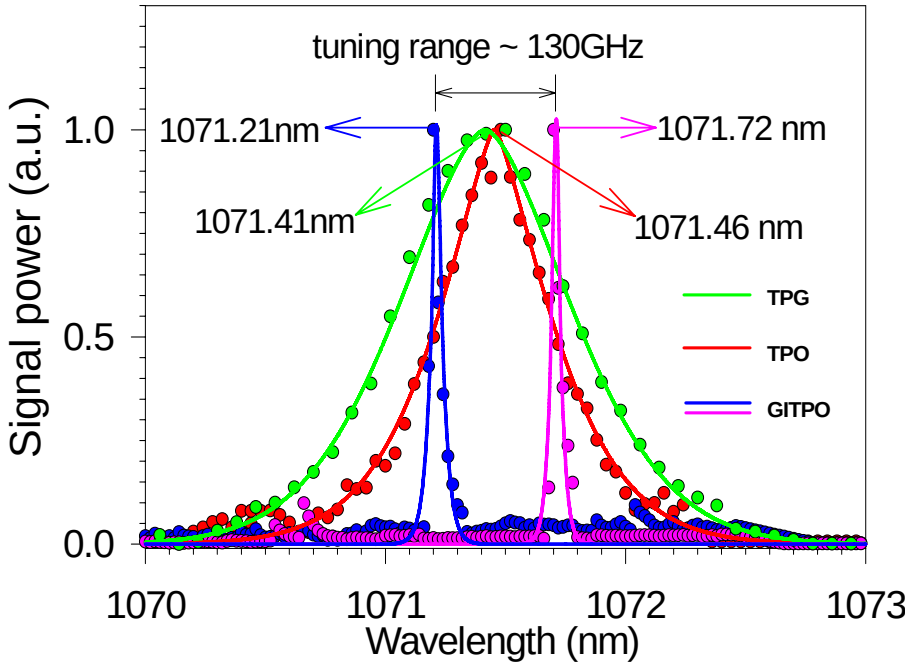


(b)

**Fig. 3-3** (a) The signal pulse width of the GITPO (blue curve) is slightly longer than that of the TPG (green curve). (b) The linewidths of the TPG (green color), TPO (red color), and GITPO (blue and pink colors) were measured to be 213, 134, and 12 GHz, respectively. The signal-wave spectrum of the GITPO was tuned over 130 GHz by rotating a 0.6-mrad angle in mirror M2.

While keeping the pump energy at 4.4 mJ and signal wavelength at 1071.45 nm, we measured the THz wavelength by using the scanning Fabry-Perot etalon between the two off-axis parabolic mirrors. Figure 3-4 shows the THz wave detected by the 4K Si bolometer versus the etalon gap. The solid curve is an Airy function fitted to the experimental data. Although the finesse of the spectrometer is not high enough for directly resolving the actual linewidth of the THz wave, the characteristic period of the transmission curve clearly shows a THz wavelength of 164 μm.

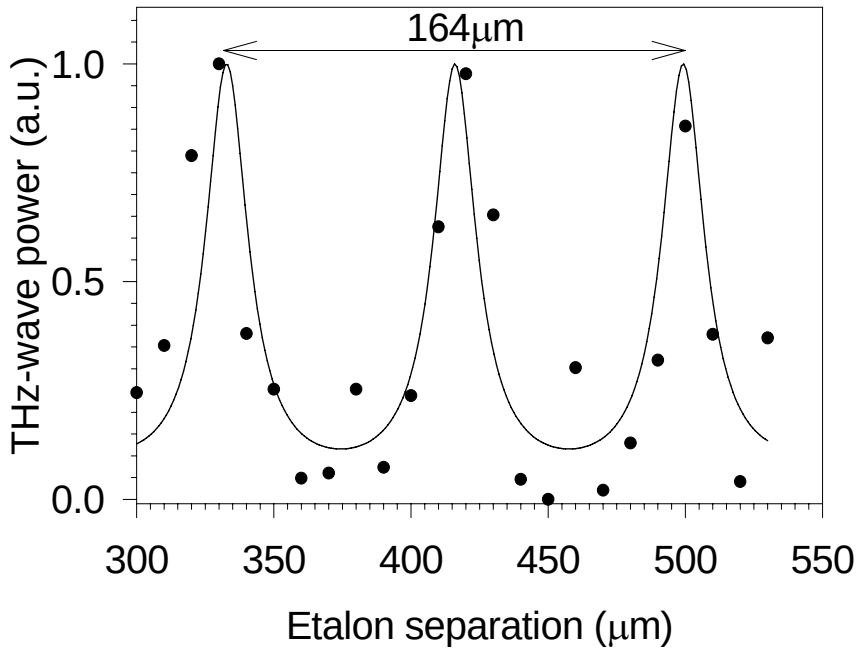


**Fig. 3-4** The measured THz-wave transmission power (filled dots) versus the etalon gap. The solid curve is an Airy function fitted to the experimental data. A THz wavelength of 164 μm can be determined from periodicity of the fitting curve.

The diffraction angle of the THz wave in the $LiNbO_3$ planar waveguide is about 10°. Therefore the 1-mm thick, 45-mm long $LiNbO_3$ crystal indeed served as a waveguide for the THz wave. In a slab waveguide, the maximum number of THz modes can be estimated from the expression $m_{\max} = 2t(n_T^2 - 1)^{1/2} / \lambda_T$, where $t$ and $\lambda_T$ are the waveguide thickness and the THz wavelength, respectively [14]. The maximum number of the waveguide modes in the 1-mm-thick $LiNbO_3$ waveguide is 63 for $n_T$ = 5.25 at the 164-μm wavelength. However, not all waveguide modes but only those phase-matched ones with mode field distributions well overlapped with the

pump mode can grow to some appreciable energy level [9]. Since the $TM_0$ mode has the largest overlap integral with the filtered $TEM_{00}$ pump beam, it is most likely that the $TM_0$ mode extracts most the parametric gain and is the dominant mode in such a multimode waveguide.

To estimate the THz-wave conversion efficiency of the GITPO inside the $LiNbO_3$ planar waveguide, we consider the pump intensity of 140 MW/cm$^2$ and the output signal-wave energy of 219 μJ at 4.4-mJ pump energy. In the theoretical limit [15], the optical-to-THz-wave conversion efficiency of the GITPO can be calculated to be ~$2.8\times10^{-5}$, corresponding to ~123 nJ THz-wave energy in $LiNbO_3$. In the calculation, we have used the absorption coefficient and the nonlinear coefficient of 30 cm$^{-1}$ and 228 pm/V, respectively, for $LiNbO_3$ at 164 μm. Given the large absorption coefficient of $LiNbO_3$, most THz-wave energy did not exit the $LiNbO_3$ crystal. Since the purpose of this work is to demonstrate the low threshold and narrow linewidth of a TPO, we simply used an existing Si grating and detected the THz wave along the more convenient 2$^{nd}$-order diffraction direction. We estimated ~1.2-pJ THz-wave energy entering the detection cone of out Si bolometer. With a more optimized output coupling scheme, the extraction of the THz-wave energy could be greatly improved [4].

## 3-4 Conclusions

We have demonstrated low pump thresholds for an externally pumped TPO and a GITPO by using a $LiNbO_3$ planar waveguide as the parametric gain medium. The low pump threshold resulted from waveguide confinement of the generated THz wave and thus better overlap between the mixing waves. The GITPO shows an additional advantage of a greatly narrowed spectral output. The measured threshold energy and intensity of the GITPO were 2.2 mJ and 70 MW/cm$^2$, respectively, which are approximately 10 times lower than the previously reported values [8, 10]. At the pump energy of 4.4 mJ (two times above threshold), the overall parametric conversion efficiency of the GITPO is about 5%. The intra-cavity grazing-incidence grating of the GITPO effectively reduced the signal and thus the THz-wave linewidth by 11 times from the value of the TPO. We measured a 12-GHz output linewidth for the

GITPO. By rotating the angle of the resonator mirror next to the grating of the GITPO, we were able to fine tune the output frequency of the GITPO by 130-GHz without changing the pump direction relative to the crystal orientation. Our scanning Fabry-Perot etalon confirmed a THz wavelength of 164 μm from the GITPO. The accomplishment of this work is a major step toward realizing low threshold and narrow-linewidth THz-wave sources.

## References


1 K. Imai, K. Kawase, J. Shikata, H. Minamide, and H. Ito, "Injection-seeded terahertz-wave parametric oscillator," Appl. Phys. Lett. **78**, 1026-1028 (2001).

2 A. Sato, K. Kawase, S. Wada, and H. Ito, "Tabletop terahertz-wave parametric generator using a compact, diode-pumped Nd:YAG laser," Rev. Sci. Instrum., **72**, 3051-3054 (2001).

3 K. Kawase, M. Sato, T. Taniuchi, and H. Ito, "Coherent tunable THz wave generation from $LiNbO_3$ with monolithic grating coupler," Appl. Phys. Lett. **68**, 2483-2485 (1996).

4 K. Kawase, J. Shikata, and H. Ito, "Terahertz wave parametric source," J. Phys. D: Appl. Phys. **35**, R1-R14 (2002).

5 S. Ohno, R. Guo, H. Minamide, and H. Ito, "High-resolution spectroscopy using a ring-cavity THz-wave parametric oscillator and Fabry-Perot interferometer," in *the 7th Pacific Rim Conference on Lasers and Electro-Optics (CLEO/Pacific Rim 2007)*, Technical Digest (CD), paper WP_124.

6 H. Minamide, K. Kawase, K. Imai, A. Sato, and H. Ito, "A novel tuning method for a ring-cavity THz-wave parametric oscillator," in *Conference on Lasers and Electro-Optics/Quantum Electronics and Laser Science and Photonic Applications Systems Technologies*, (Optical Society of America, 2001), paper CThJ3.

7 T. J. Edward, D. Walsh, M. B. Spurr, C. F. Rae, M. H. Dunn, and P. G. Browne, "Compact source of continuously and widely tunable terahertz radiation," Opt. Express **14**, 1582-1589 (2006).

8 A. C. Chiang, T. D. Wang, Y. Y. Lin, S. T. Lin, H. H. Lee, Y. C. Huang, and Y. H. Chen, "Enhanced terahertz-wave parametric generation and oscillation in lithium niobate waveguides at terahertz frequencies," Opt. Lett. **30**, 3392-3394 (2005).

9 A. C. Chiang, T. D. Wang, Y. Y. Lin, S. T. Lin, H. H. Lee, Y. C. Huang, and Y. H. Chen, "Enhanced terahertz-wave parametric generation and oscillation in lithium niobate waveguides at terahertz frequencies," Opt. Lett. **30**, 3392-3394 (2005).

10 Y. Sasaki, Y. Suzuki, K. Suizu, H. Ito, S. Yamaguchi, and M. Imaeda, "Surface-emitted terahertz-wave difference-frequency generation in periodically poled lithium niobate ridge-type waveguide," Jpn. J. Appl. Phys. **45**, L367-L369 (2006).

11 K. C. Harvey and C. J. Matt, "External-cavity diode laser using a grazing-incidence diffraction grating," Opt. Lett. **16**, 910-912 (1991).

12 Y. Y. Lin, S. Y. Chen, A. C. Chiang, R. Y. Tu, Y. C. Huang, Y. F. Chen, and Y. H. Chen, "Single-longitudinal-mode, tunable dual wavelength, CW Nd:$YVO_4$ laser," Opt. Express **14**, 5329-5334 (2006).

13 C. S. Yu and A. H. Kung, "Grazing-incidence periodically poled LiNbO3 optical parametric oscillator," J. Opt. Soc. Am. B **16**, 2233-2238 (1999).

14 B. E. A. Saleh and M. C. Teich, *Fundamentals of Photonics*, 251 (Wiley, 1991).

15 S. S. Sussman, "Tunable light scattering from transverse optical modes in lithium niobate," Microwave Lab. Report No. 1851, (Stanford University, Stanford, Calif., 1970).

# Chapter 4 Forward and Backward Terahertz-wave Difference-frequency Generations from Periodically Poled Lithium Niobate

In chapter 4, we report terahertz-wave generation in the wavelength range of 190~210 and 457~507 μm from forward and backward difference frequency generations, respectively, in a 3.2-cm long multi-grating periodically-poled lithium niobate crystal (PPLN). The grating period of the PPLN crystal varies from 63 to 70 μm in 1-μm increments. The extraordinary refractive index of lithium niobate in the THz-wave range was precisely deduced from the quasi-phase-matching condition of the difference frequency generations.

## 4-1 Introduction

A terahertz (THz) wave source could be useful for applications such as spectroscopy, noninvasive imaging, and drug detection [1, 2, 3, 4]. For incoherent THz radiation, ultra-fast laser gated optical rectification [5] and photoconductive switching [6] are two widely adopted schemes. For coherent THz radiation, there are also a number of approaches. For example, a free electron laser is capable of generating high-power and broadly tunable THz radiation [7]; however, its large size and high cost have restricted its use to a limited number of researchers. The THz quantum-cascade laser [ 8 ] is another type of coherent THz source, but room-temperature, high-power operation of such a source is not yet demonstrated. Optical parametric down conversion has been a popular scheme for generating coherent THz waves at room temperature. For example, THz-wave generation from polariton scatting in lithium niobate ($LiNbO_3$), pioneered by Pantell [9], has been greatly improved by Ito [10, 11, 12] in the past 10 years. With the non-collinear phase matching condition, the THz wave in $LiNbO_3$ is emitted at about 65° from the pump-beam direction and is often trapped inside the crystal due to the total internal reflection. Specially arranged Si prisms or gratings have been used to couple out the THz power from the $LiNbO_3$ crystal [12].

Usually, collinear phase-matching is the preferred configuration for a nonlinear frequency conversion process, because it provides the longest interaction length and more efficient power extraction from a normal-incidence crystal face. Optical rectification using a fs pump laser in a quasi-phase-matched (QPM) [13] nonlinear optical material can also generate forward and backward multi-cycle THz radiations [14, 15, 16]. The mechanism of the THz-wave generation is understood as a special case of difference frequency generation in that two Fourier components of the fs laser pulse perform wave mixing [17]. However in the collinear configuration the generated THz-wave quickly walks away from the short pump pulse and is mostly absorbed before existing the nonlinear optical material. On the other hand, the conventional collinearly phase-matched difference frequency generation using two coherent long-pulse pump components promises much more power and better coherence for the generated THz wave [18].

Previous theoretical studies [18, 19] have shown that both forward and backward difference frequency generations for THz waves can be conveniently arranged with a collinearly phase matched configuration in periodically poled lithium niobate (PPLN). The backward scheme is particular interesting in that mirror-less oscillation can be achieved with a sufficiently large pump intensity [20]. It is hoped that successful demonstration in the mid-infrared spectrum [21] could be extended to the THz-radiation spectrum. However, a THz backward optical parametric oscillator (OPO) would have a much higher pump threshold due to the relatively strong absorption and diffraction of the THz wave in a nonlinear optical material. Nonetheless, backward difference frequency generation of THz waves was demonstrated in a birefringence-phase-matched GaSe crystal [22]. Quasi-phase-matched GaAs could be a good candidate for demonstrating a THz backward OPO, but the technique for fabricating a large-aperture, low-loss, long enough QPM GaAs is not yet available. In this paper, we demonstrate, to the best of our knowledge, the first forward and backward difference frequency generations of coherent THz waves from a multi-grating PPLN crystal. From the quasi-phase-matching condition, we precisely deduced the refractive index of $LiNbO_3$ in the THz spectrum.

## 4-2 Experimental Configuration of the Forward and Backward THz-wave Difference-frequency Generators

Figure 4-1 shows the experimental setup of the forward and backward THz difference frequency generations. A kHz-linewidth distributed-feedback diode laser (DFBDL) at 1538.98 nm and a MHz-linewidth external-cavity diode laser (ECDL) tunable between 1510 and 1610 nm provide the seed components to the first-stage Erbium-doped fiber amplifier (EDFA) and the second-stage pulsed optical parametric amplifier (OPA) for the THz difference frequency generations in the PPLN difference frequency generator (PPLN DFG). The EDFA boosts up the CW diode-laser powers to about 70 mW. A passively Q-switched Nd:YAG laser at 1064 nm pumps the OPA using a PPLN crystal as the gain medium. The PPLN-OPA crystal has a 0.78-mm thickness, 45-mm length, and 29.6-μm QPM period. The OPA pump laser generates 70-μJ pulse energy in a 500-ps pulse width repeating at a 1 kHz rate. The pump laser is focused to a waist radius of 166 μm at the center of the PPLN-OPA crystal. At 101$^{o}$C, the PPLN OPA has a 12-nm or 1.6-THz bandwidth so this OPA can simultaneously amplify the two seed components from the diode lasers. After the OPA, each of the two seed components is amplified to ~8.5-μJ pulse energy in a 400-ps pulse width for pumping the THz PPLN DFG. The one-to-one power ratio in the two pump components maximizes the output power of the difference frequency generation in the low-conversion limit. The two idler waves of the OPA near 3.3 μm were completely absorbed by the BK7 substrate of the dichroic mirror (HR @1064 nm and HT @1550 nm). The two pump components near 1.5 μm were focused by a $f$ = 7.5-cm focusing lens to a 130 μm waist radius at the center of a multi-grating PPLN-DFG crystal for performing the forward and backward THz difference frequency generations. One major advantage of this broadband two-stage amplifier system is that the spatial and temporal overlap of the two pump components of the PPLN DFG is automatically achieved. In addition, the THz frequency can be easily tuned by varying the relative frequency between the two seed diode lasers. The 400-ps pulse width of the OPA output, however, gives a walkoff distance between the optical and THz pulses comparable to the 3.2-cm crystal length of the PPLN DFG.

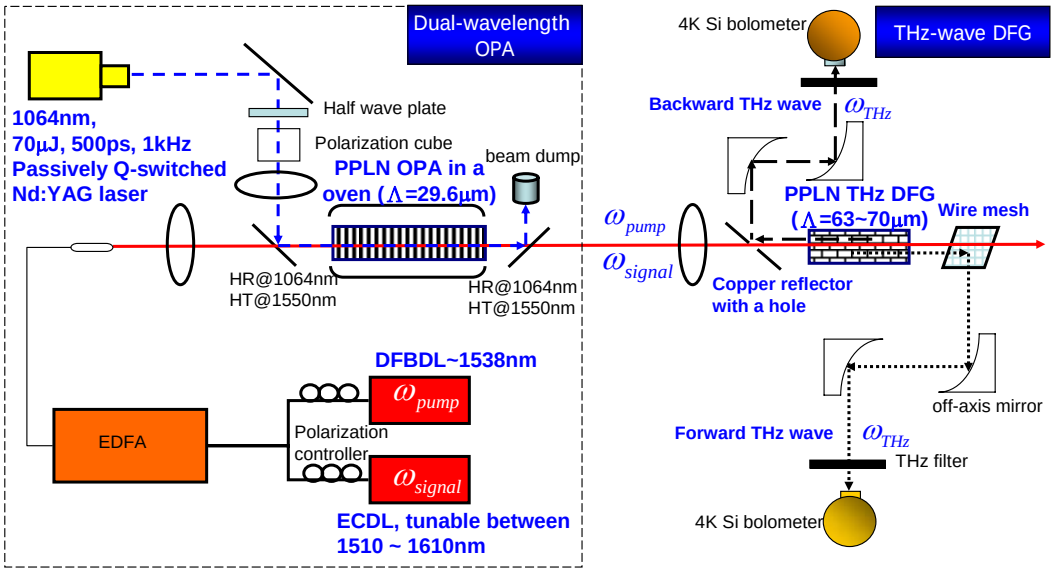


**Fig. 4-1** Setup of the collinearly quasi-phase-matched forward and backward THz difference frequency generations in a multi-grating PPLN crystal. The two-stage amplifier, marked by a dashed-line box, generates 17-μJ pump energy in a 400-ps pulse width with two frequency components from the seeding DFBDL and the ECDL. The 17-μJ pump energy is injected to into the PPLN DFG for generating coherent THz radiation. The frequency tuning of the THz wave is achieved by varying the frequency difference between the two diode lasers matched to the QPM conditions of the DFG PPLN. (HR: high reflection, HT: high transmission, OPA: optical parametric amplifier, DFG: difference frequency generator, FP: Fabry-Perot spectrometer, ECDL: external-cavity diode laser, DFBDL: distributed-feedback diode laser, EDFA: Erbium-doped fiber amplifier.)

The DFG employed a multi-grating PPLN crystal with a 0.78-mm thickness. The PPLN crystal consists of 8 parallel QPM gratings with 63, 64, 65, 66, 67, 68, 69, and 70-μm domain periods. The end faces of the PPLN crystal were coated with anti-reflection dielectric layers at the two pump wavelengths (Reflectance <0.5%).

The forward THz wave was largely separated from the pump components by using a wire mesh in the down stream of the PPLN DFG. The wire mesh contains 45 μm × 45 μm square apertures with a 54% filling factor. The transmittance of the wire mesh is 14% and 84% for incident waves near 200 and 1.55 μm, respectively. The residual pump laser reflected from the wire mesh is completely blocked by a 3-mm thick Ge filter and a high-density polyethylene filter in front of the bolometer. The backward THz wave was extracted by using an optically polished 3.5 cm × 3.5 cm square copper reflector placed 3 cm in front of the multi-grating PPLN crystal. The

copper reflector has a 5-mm diameter hole for transmitting the two pump components, but reflects nearly 94% of the THz wave incident on it. The counter-propagating configuration of the pump and THz waves in the backward THz-wave DFG provides a pump-free background for measuring the THz wave. When taking data, we scanned the wavelength of the ECDL and read the THz-wave signal from a 4K Si bolometer. When the ECDL wavelength is tuned to the quasi-phase-matching condition of the forward or backward difference frequency generation, the bolometer registers a large THz-wave signal. The bolometer signal fell back to the noise level when we blocked any of the two pump components, so generation of the forward and backward THz waves was unambiguously confirmed.

## 4-3 Experimental Results

It can be shown from the plane-wave model that the phase-tuning curve of a highly lossy forward or backward THz-wave DFG has a Lorentzian line shape given by

$$I_{THz} \propto \left| j\Delta kL + \frac{\alpha_{THz}}{2} L \right|^{-2} \tag{4-1}$$

where $I_{THz}$ is the intensity of the THz wave, $\Delta k$ is the wave-vector mismatch, $L$ is the length of the nonlinear material, $\alpha_{THz}$ is the power attenuation coefficient at THz frequencies, and $j = \sqrt{-1}$ is the imaginary unit. Figure 2 shows the forward THz phase-tuning curves measured by the bolometer. The solid curves are the best fits of the Lorentzian function in Eq. (4-1). We deduced the phase-matched wavelength of the THz radiation $\lambda_{THz}$ from the frequency conservation law, $1/\lambda_p - 1/\lambda_s = 1/\lambda_{THz}$, where $\lambda_p$ and $\lambda_s$ are the short- and long-wavelength pump components for the DFG, respectively. In Fig. 4-2 (a), the phase-matched THz-radiation wavelengths were found to be 191.6, 194.4, 197.1, 199.6, 202.4, 205.0, and 206.8 μm, corresponding to the PPLN grating periods of 63, 64, 65, 66, 67, 68, and 69 μm, respectively. The best signal-to-noise ratio in the tuning curves is more than 10. The measurements were done in a laboratory atmosphere without dry-$N_2$ purge. As shown by Fig. 4-2 (b), the

THz wave generated from the 70-μm grating near 211.5 μm was strongly absorbed by the ambient water vapor [23]. We also verified the THz radiation by directly measuring its wavelength using a scanning Fabry-Perot spectrometer. The spectrometer consists of two parallel pieces of the wire mesh with a 2.5-μm scanning step along the longitudinal direction. A THz-radiation wavelength of 197.5 μm was confirmed at the output of the 65-μm period PPLN, which is in good agreement with the wavelength deduced from the frequency conservation law.

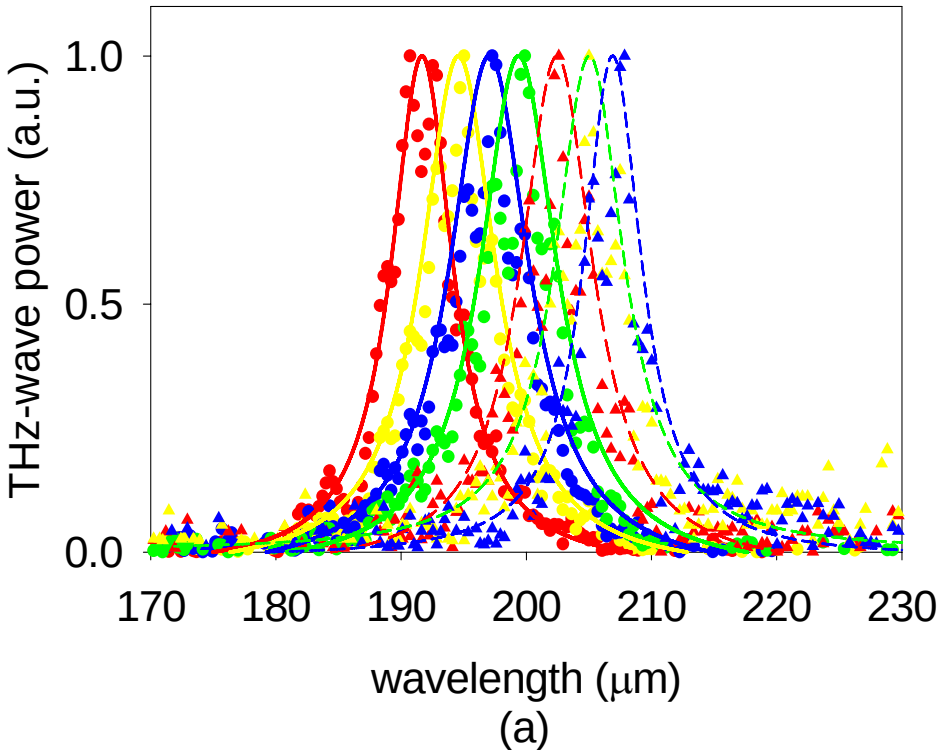

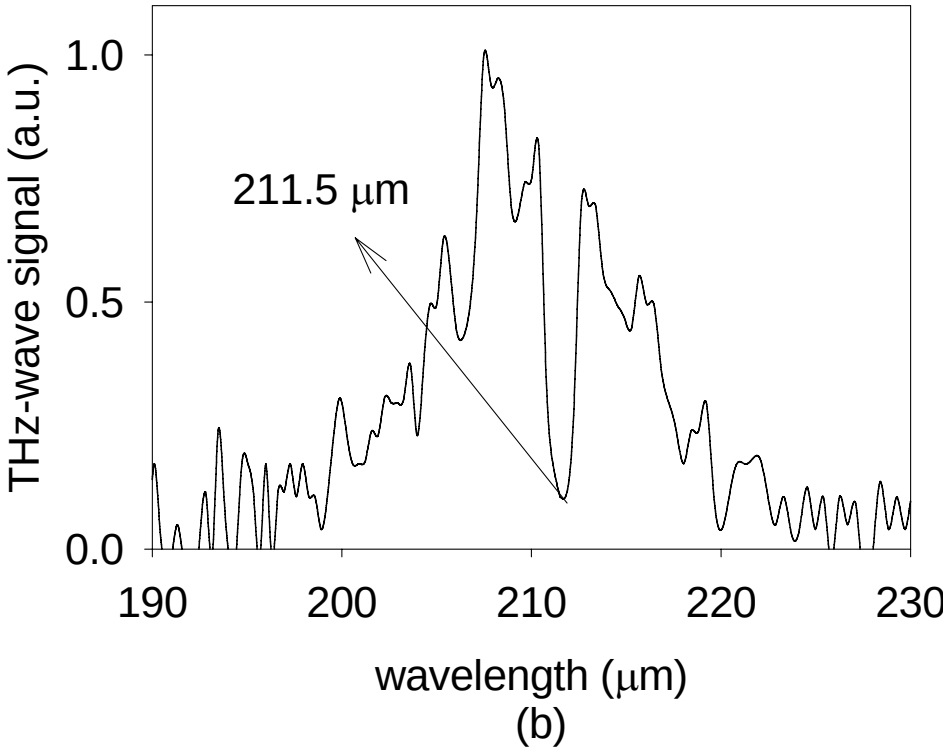


**Fig. 4-2** (a) Forward THz-wave phase-matching curves measured by the 4K Si bolometer for the PPLN gratings with 63, 64, 65, 66, 67, 68 and 69-μm periods. The solid curves are the best fits of the Lorentzian function in Eq. (4-1). (b) When taking the phase matching cure for the 70-μm period PPLN DFG, we found absorption of ambient water vapor near 211.5 μm [25].

The bolometer was specified with 100% quantum efficiency at 200 μm. From the bolometer signal, we estimated about 10-fJ THz-wave energy entering the detection cone of the bolometer. Considering the 54, 35, 72% transmittances at PPLN output face, the Ge filter, and the bolometer window, respectively, and the fast diffraction of the THz, we obtain 0.37 pJ energy of THz radiation inside the PPLN crystal.

While fixing the wavelength of the DFBDL at 1538.43 nm, we continued to scan the ECDL wavelength and read the backward THz-wave signal from the 4K Si bolometer. In Fig. 3, we plot the backward DFG tuning curves measured by the bolometer. The phase-matched THz-radiation wavelengths were found to be 456.7, 463.8, 470.2, 477.7, 484.6, 492.6, 498.8, and 507.3 μm, corresponding to the PPLN grating periods of 63, 64, 65, 66, 67, 68, 69, and 70 μm, respectively. The measurements were also done in a laboratory atmosphere without dry-$N_2$ purge. For

those measurements, the best signal-to-noise ratio in the tuning curves is also about 10.

In this experiment, the pump power for the backward THz DFG was about 2-3 orders of magnitudes lower than that for most THz-wave forward difference frequency generation in $LiNbO_3$. By assuming 100% quantum efficiency of our Si bolometer for the backward THz photons between 450~500 μm, we estimate ~6 fJ energy of the backward THz wave entering the detection cone of the bolometer. The backward THz wave was emitted from the input face of the PPLN crystal with a radiation area approximately equal to the pump laser area. Since the 130-μm pump laser radius is several times less than the radiation wavelength, the THz wave appears to radiate from a point source from the PPLN end face covering a nearly 2π solid angle. The first $f$ = 76-mm, 2″-aperture off-axis parabolic mirror was responsible for collecting the THz radiation into the bolometer, which was placed ~7 cm from the PPLN input face due to the space constraint in our setup. This suggests that, with our current setup, only a very small fraction of the THz-wave energy collected into the sensor area of the bolometer. Further taking into account the ~50% Fresnel reflection at the PPLN surface, we conclude a minimum of 56-fJ energy of the backward THz wave was generated in the PPLN. Further improvements on the detection scheme and the detector calibration are needed to understand the conversion efficiency of this backward THz difference frequency generation. In addition, the short 400-ps pump pulse lengths only allow 200-ps buildup time for the backward-propagating THz wave in the highly absorptive PPLN. This means the effective gain length of our backward THz DFG is only 1.2 cm, given a THz refractive index of ~5.

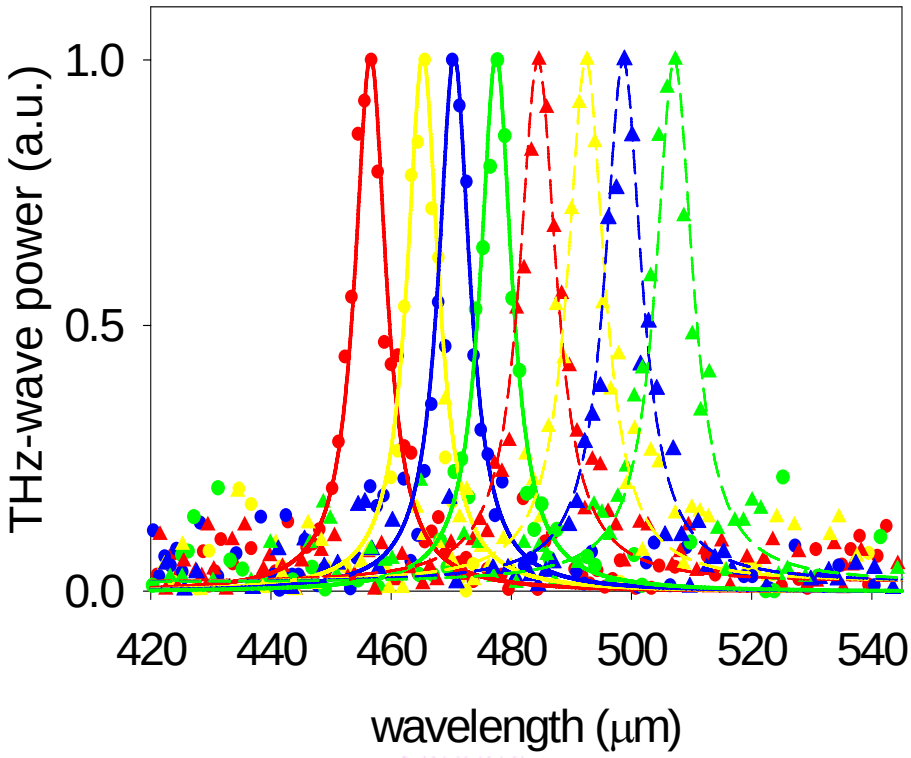


**Fig. 4-3** Backward THz-wave phase matching curves measured by the 4K Si bolometer for the PPLN with 63, 64, 65, 66, 67, 68, 69 and 70-μm periods. The solid curves are the best fits of the Lorentzian function in Eq. (4-1).

Table 4-1 summaries the generated THz wavelengths and deduced refractive indices of the forward and backward THz difference frequency generations. For the forward THz-wave generation, the data for the 70-μm PPLN grating period is not available (NA) due to water absorption at the generated wavelength. The refractive index can be deduced from the QPM condition $n_p/\lambda_p - n_s/\lambda_s - 1/\Lambda_{PPLN} = \pm n_{THz}/\lambda_{THz}$ with known material dispersion at the optical frequencies, where the + and – signs denote the forward and backward processes, respectively, $\Lambda_{PPLN}$ is the PPLN grating period, and $n$ is the refractive index. For the PPLN DFG, $n_{THz}$ is the extraordinary refractive index seen by the THz radiation.

Figures 4-4(a, b) show the measured extraordinary refractive indices (dots) versus the forward and backward THz-wave wavelengths, respectively. For comparison, we also overlay on the same plots the fitting curves of the THz-wave refractive index from Refs. [24, 25]. In Fig. 4-4(a), the fitting curve from Ref. [24] matches reasonably well to our measured data. In Fig. 4-4(b), the experimental data are in a good agreement with Ref. [25]. Usually it is relatively difficult to precisely

measure the refractive index of a material at the THz frequency. The quasi-phase-matched difference-frequency generations offer a convenient and precise way of characterizing material dispersion at THz frequencies.

**Table 4-1.** Summary of the forward and backward THz difference frequency generations

| Forward THz-wave Generation | | | | | | | | |
|---|---|---|---|---|---|---|---|---|
| PPLN period (μm) | 63 | 64 | 65 | 66 | 67 | 68 | 69 | 70 |
| Measured THz wavelength (μm) | 191.6 | 194.4 | 197.1 | 199.6 | 202.4 | 205.0 | 206.8 | NA |
| Deduced extraordinary refractive index | 5.2243 | 5.2203 | 5.2152 | 5.2064 | 5.2039 | 5.1976 | 5.1794 | NA |
| Backward THz-wave Generation | | | | | | | | |
| Measured THz wavelength (μm) | 456.7 | 463.8 | 470.2 | 477.7 | 484.6 | 492.6 | 498.8 | 507.3 |
| Deduced extraordinary refractive index | 5.0663 | 5.0641 | 5.0512 | 5.0559 | 5.0494 | 5.0609 | 5.0456 | 5.0638 |

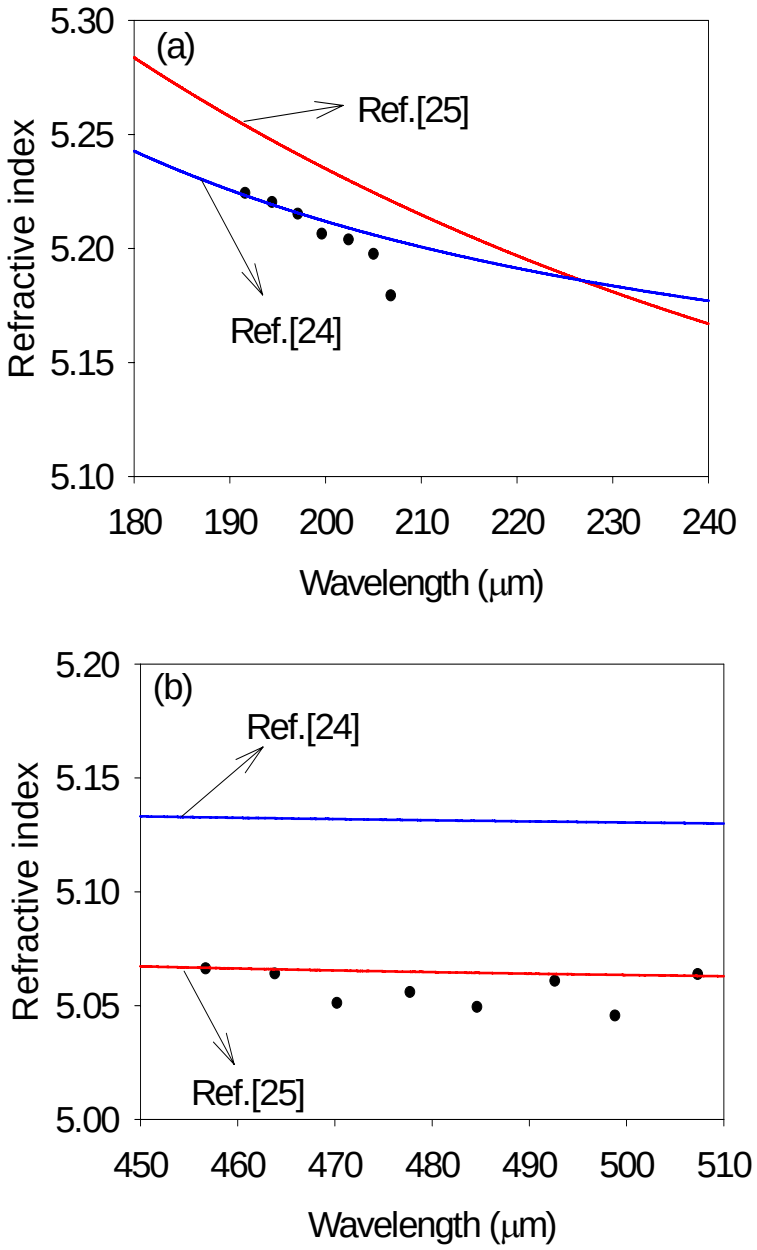


**Fig. 4-4** The THz extraordinary refractive indices deduced from the (a) forward and (b) backward THz-wave difference frequency generations. The fitting curves from Refs. [24, 25] are also shown for comparison.

## 4-4 Discussions and Conclusions

Although the QPM technique holds some promise to increase the gain length for parametric THz-wave generation from $LiNbO_3$, future work is necessary to make a direct comparison between the collinear and non-collinear phase-matching schemes under the same pump power and radiation wavelength. As an attempt to achieve backward parametric oscillation, we also used a single high-power source to pump the

PPLN crystal but only generated high-order phase-matched forward mid-infrared radiation. Apparently, in our PPLN crystal, the net gain of the backward parametric process for THz-wave generation is much lower than that of the forward parametric process for mid-infrared generation. Forced nonlinear dipole radiation with a more intense seed signal for the DFG could be an approach to achieve backward-wave oscillation at the THz frequencies.

We have demonstrated collinearly quasi-phase-matched forward and backward DFG for generating THz waves near 200 and 500 μm, respectively, from a multi-grating PPLN crystal with a pump power 2~3 orders of magnitude lower than that for most THz-wave generations using $LiNbO_3$. Owing to the narrow linewidths of the two seed diode lasers, the generated THz waves are expected to be transform limited. We estimated that about 0.37 and 0.056 pJ energies of the forward and backward THz waves, respectively, were generated in the PPLN crystal. Owing to the vast difference in the optical and THz refractive indices in $LiNbO_3$, the 400-ps pump pulse width could have limited the effective gain lengths for both the forward and backward DFG's. We also found from a plane-wave model that the ideal power ratio for the two pump powers deviated from the one-to-one ratio in a pump-depleted, high-gain DFG. We expect to generate much more THz-wave energy by using more intense pump sources with a longer pulse length and a more optimized power ratio in our future work. Further improvements on collecting the quickly diffracted THz wave and calibrating the THz detector are among our next efforts for understanding and maximizing the efficiency of the THz difference frequency generations. Nonetheless, the QPM forward and backward difference frequency generations are very effective for measuring the refractive index of $LiNbO_3$ at the THz frequencies. What has been accomplished in this work is potentially an important step toward the realization of a tunable, low-pump-power coherent THz source.

## References


1 C. Rønne, P. Åstrand, and S. R. Keiding, "THz spectroscopy of liquid $H_2O$ and $D_2O$," Phys. Rev. Lett. **82**, 2888-2891 (1999).

2 E. Knoesel, M. Bonn, J. Shan, and T. F. Heinz, "Charge transport and carrier Dynamics in Liquids Probed by THz Time-Domain Spectroscopy," Phys. Rev. Lett. **86**, 340-343 (2001).

3 K. Kawase, Y. Ogawa, Y. Watanabe, and H. Inoue, "Non-destructive terahertz imaging of illicit drugs using spectral fingerprints," Opt. Express. **11**, 2549-2554 (2003).

4 Q. Wu, T. D. Hewitt, and X.-C. Zhang, "Two-dimensional electro-optic imaging of THz beams," Appl. Phys. Lett. **69**, 1026-1028 (1996).

5 P. R. Smith, D. H. Auston, and M. C. Nuss, "Subpicosecond photoconducting dipole antennas," IEEE J. Quantum Electron. **24**, 255-256 (1988).

6 X.-C., B. B. Hu, J. T. Darrow, and D. H. Auston, "Generation of femtosecond electromagnetic pulses from semiconductor surface," Appl. Phys. Lett. **56,** 1011-1013 (1990).

7 D. H. Levy, *Free Electron Lasers and Other Advanced Sources of Light*, National Academy Press Washington, DC, 24–31 (1994).

8 R. Köhler, A. Tredicucci, F. Beltram, H. E. Beere, E. H. Linfield, A. G. Davies, D. A. Ritchie, R. C. Iotti and F. Rossi, "Terahertz semiconductor-hetrostructure laser," Nature **417,** 156-159 (2002).

9 M. A. Piestrup, R. N. Fleming, and R. H. Pantell, "Continuously tunable submillimeter wave Source," Appl. Phys. Lett. **26**, 418-419 (1975).

10 K. Kawase, M. Sato, T. Taniuchi, and H. Ito, "Coherent THz-wave generation from $LiNbO_3$ with monolithic grating coupler," Appl. Phy. Lett. **68**, 2483-2485 (1996).

11 J. Shikata, M. Sato, T. Taniuchi, and H. Ito, "Enhancement of Terahertz-wave output from $LiNbO_3$ optical parametric oscillator by cryogenic cooling," Opt. Lett. **24**, 202-204 (1999).

12 K. Kawase, J. Shikata, ,H. Minamide, K. Imai, and H. Ito, "Arrayed silicon prism coupler for THz-wave parametric oscillator," Appl. Opt. **40**, 1423-1426 (2001).

13 J. A. Armstrong, N. Bloemergen, J. Ducuing, and P. S. Pershan, "Interactions between light waves in a nonlinear dielectric," Phys. Rev., **127**, 1918-1939 (1962).

14 Y. S. Lee, T. Meade, V. Perlin, H. Winful, T. B. Norris, and A. Galvanauskas, "Generation of narrow-band terahertz radiation via optical rectification of femtosecond pulses in periodically poled lithium niobate," Appl. Phys. Lett. **78**, 2505-2507 (2000).

15 C. Weiss, G. Torosyan, J. P. Meyn, R. Wallenstein, R. Beigang, and Y. Avetisyan, "Tuning characteristics of narrow band THz radiation generated via optical

rectification in periodically poled lithium niobate," Opt. Express **8,** 497-502 (2001).

16 N. E. Yu, C. Jung, C. S. Kee, Y. L. Lee, B. A. Yu, D. K. Ko, and J. Lee, "Backward terahertz generation in periodically poled lithium niobate crystal via difference frequency generation," Jpn. J. Appl. Phys. **46,** 1501-1504 (2007).

17 Konstantin L. Vodopyanov, "Optical generation of narrow-band terahertz packets in periodically-inverted electro-optic crystals: conversion efficiency and optimal laser pulse format," Opt. Express **14,** 2263-2276 (2006).

18 W. Shi, Y. J. Ding, N. Fernelius, K. Vodopyanov, "Efficient, tunable, and coherent 0.18-5.27-THz source based on GaSe crystal," Opt. Lett. **27**, 1454-1456 (2002).

19 Y. J. Ding and J. B. Khurgin, "A new scheme for efficient generation of coherent and incoherent submillimeter to THz wave in periodically-poled lithium niobate," Opt. Commun. **148**, 105-109 (1998).

20 S. E. Harris, "Proposed backward wave oscillation in the infrared," Appl. Phys. Lett. **9**, 114-115 (1966).

21 C. Canalias, and V. Pasiskevicius, "Mirror-less optical parametric oscillator," Nature Photonics **1**, 459-462 (2007).

22 Wei Shi, and Yujie J. Ding, "Backward parametric oscillation in second-order nonlinear medium," in *Conference on Lasers and Electro-Optics/Quantum Electronics and Laser Science and Photonic Applications Systems Technologies*, Technical Digest (CD) (Optical Society of America, 2005), paper QTuF7.

23 V. B. Podobedov, D. F. Plusquellic and G. T. Fraser, "Investigation of the water-vapor continuum in the THz region using a multipass cell," J. Quant. Spectrosc. Radiat. Transfer **91**, 287-295 (2005).

24 L. Pálfalvi, J. Hebling, J. Kuhl, Á. Péter and K. Polgár, "Temperature dependence of the absorption and refraction of Mg-doped congruent and stoichiometric LiNbO3 in the THz range," J. Appl. Phys. **97**, 123505-123511 (2005).

25 E. D. Palik, *Handbook of Optical Constants of Solids*, 695-702 (Academic, New York, 1991).

# Chapter 5 Conclusions

## 5-1 Contribution of this Dissertation

This dissertation proposes a series of tunable, ultra-low threshold, coherent terahertz-wave generation in lithium niobate ($LiNbO_3$) crystals with or without inverted domains. This study will dedicate a lot of fruitful results to spectroscopy, noninvasive imaging, and drug detection.

In Chapter 2, I observed the parametric-generation efficiency of 1.61% from 1064 nm to 1071 nm and 162 μm in a 0.5 mm thick, 45 mm long z-cut congruent $LiNbO_3$ waveguide with a pump energy of 2.2 mJ and a pump pulse width of 5.8 ns. We also measured the lowest threshold intensity of 70 MW/cm$^2$ for a 1064 nm pumped parametric oscillator resonating at 1071 nm and emitting at 162 μm using a 1 mm thick, 45 mm long $LiNbO_3$ waveguide. The major contribution in this chapter is I firstly demonstrated waveguide-enhanced parametric conversion at terahertz (THz) frequency from z-cut congruent $LiNbO_3$ wafers of various thicknesses.

In Chapter 3, I reported a lowest-threshold, narrowest-line THz-wave parametric oscillator (TPO) with an intra-cavity grazing-incidence grating and a 1 mm thick, 45 mm long $LiNbO_3$ planar waveguide. When pumped by an actively Q-switched Nd:YAG laser, the threshold energy and intensity of the parametric oscillator were about 2.2 mJ and 70 MW/cm$^2$ (the lowest pump intensity in record), respectively. The linewidths of the output THz wave were 12 and 134 GHz with and without the intra-cavity grating, respectively. The energy conversion efficiency, the pump threshold, and the THz linewidth are the highest, lowest, and narrowest among all the reported values for similar devices.

In Chapter 4, I demonstrated THz-wave generation in the wavelength range of 190~210 μm and 457~507 μm from forward and backward difference frequency generations, respectively, in a 3.2 cm long multi-grating periodically poled lithium niobate (PPLN) crystal. The grating period of the PPLN crystal varies from 63 μm to 70 μm in 1 μm increments. The extraordinary refractive index of $LiNbO_3$ in the THz-wave range was precisely deduced from the quasi-phase-matching condition of

the difference frequency generations. My work is the first demonstration of forward and backward THz-wave generations from collinearly phase-matched difference frequency mixing in PPLN.

What this dissertation has accomplished is potentially an important step towards the realization of a tunable, low-pump-power, high-efficiency coherent THz source.

## 5-2 Future Work

***PPLN nonlinear semi-waveguide***

THz-wave difference-frequency generation in $LiNbO_3$ has a great advantage in generating coherent THz-wave radiation; thus, increasing the conversion efficiency is not conventional. However, this kind of configuration has some major difficulties. First is the non-collinear phase matching condition, in which the THz wave in $LiNbO_3$ is emitted at about 65° from the pump-beam direction. In addition, it limits the interaction length. Second is the fast diffraction of the THz wave in the bulk crystal. In the $LiNbO_3$ crystal, the absorption coefficient is tremendously large (74 $cm^{-1}$ at 150 μm) [1]. The generated THz-wave quickly walks away from the pump area and is mostly re-absorbed before existing the nonlinear optical material. Due to the above-mentioned difficulties, increasing the conversion efficiency is tough task.

Generally, to overcome the above-mentioned problems, collinear phase-matching is the straightforward configuration for a nonlinear frequency conversion process because it provides the longest interaction length and more efficient power extraction from a normal-incidence crystal face. Therefore, a quasi-phase-matched (QPM) [2] crystal is a popular technique that can provide additional grating vector to compensate for the phase-miss-matched problems of the interaction waves in the collinear direction.

A THz waveguide is known to confine the THz radiation and enhance the parametric conversion efficiency. This has also been confirmed by some experimental and theoretical reference papers [3, 4]. By taking advantage of the THz waveguide, we propose significant improvements by using a nonlinear optical THz waveguide with collinear phase-matched THz different-frequency generation configuration in a PPLN crystal.

To reduce the diffraction loss, we plan to replace the slab nonlinear semi-waveguide with the rectangular nonlinear semi-waveguide in the PPLN material (see Fig. 5-1(a)). Figure 5-1(b) shows the schematic diagram of the THz difference-frequency generator (DFG) with the pump wave at 1538.98 nm, the signal wave at 1550.1 nm, and the generated THz wave at 200 μm. The DFG laser system starts from a kHz-linewidth distributed-feedback diode laser at 1538.98 nm and from a MHz-linewidth external-cavity diode laser tunable between 1510 nm and 1610 nm. To achieve this end, we first sent the two seed lasers into an Erbium-doped fiber amplifier followed by a pulsed optical parametric amplifier. One of the diode laser wavelengths can be tuned so that the phase-matching THz wavelength can be deduced.

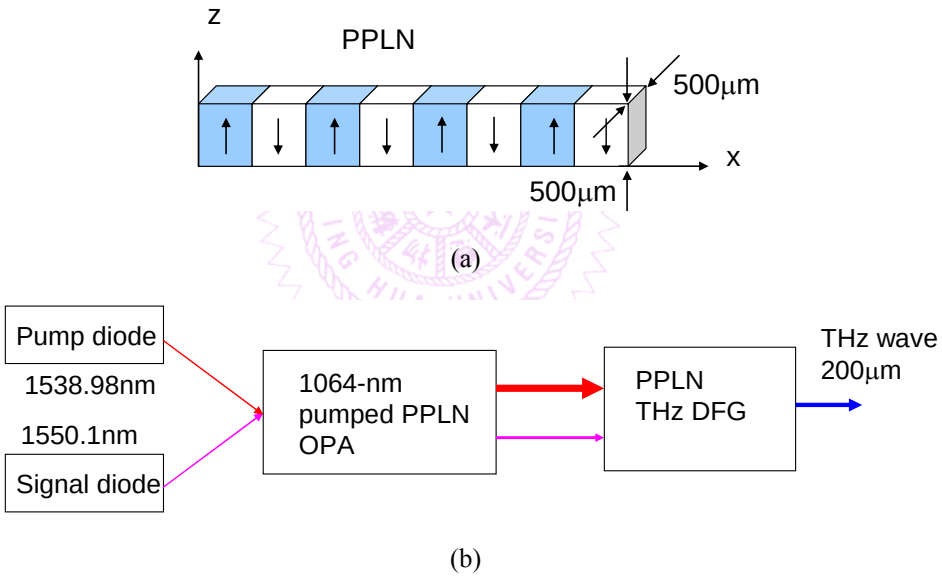


**Fig. 5-1** (a) A PPLN nonlinear semi-waveguide (guiding the THz wave but not the optical pump waves) aims to improve THz-wave conversion efficiency; (b) The schematic diagram of THz-wave generation pumped by two near 1.5 μm lasers.

Figure 5-2(a) shows the simulation of the energy flow from the pump wave to the signal wave with the initial pump and signal powers of 32 kW and 14 kW. Figure 5-2(b) reveals that the saturated THz conversion efficiency is $3.7\times10^{-4}$ at a PPLN crystal length of 1.8 cm. The saturated THz conversion efficiency is two orders of magnitude higher than the ones shown in Chapter 4. In the ideal limit, the watt-level peak power from this configuration can be demonstrated.

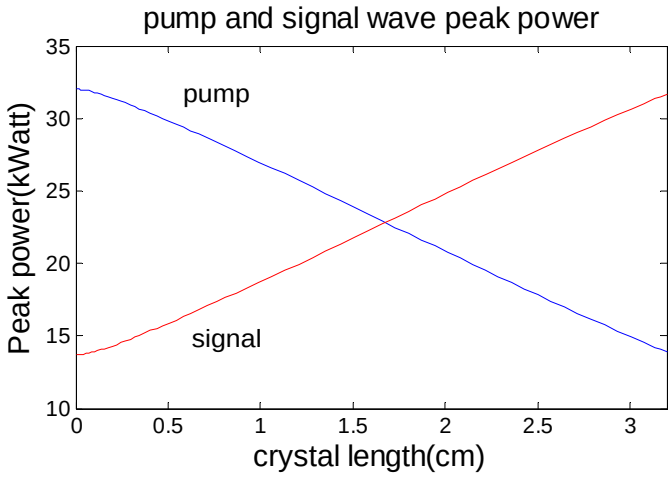


(a)

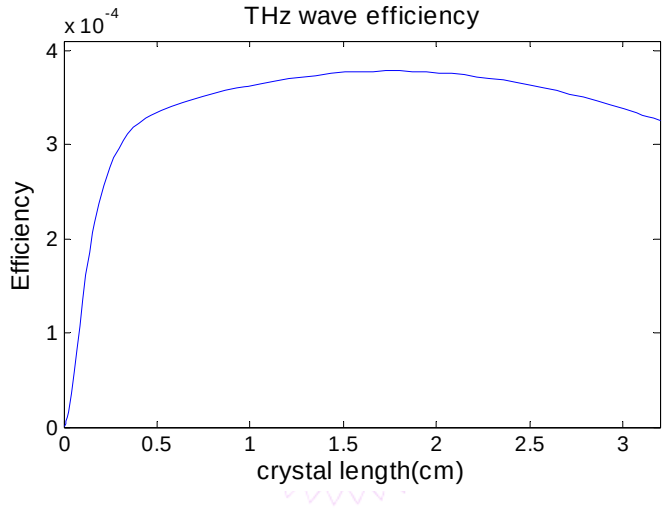


(b)

**Fig 5-2** (a) Simulation of the pump/signal power flows versus crystal length; (b) THz-wave conversion efficiency versus crystal length. Due to the fast diffraction of the THz wave, the previously demonstrated efficiency was only about $10^{-7}$.

### *New materials and methods for THz-wave generation*

The efficient generation of the THz wave is very important to applications in many fields such as medical imaging, noninvasive material and structure detections, and communications [5, 6, 7]. Considering the advantages of its large nonlinear coefficient and low absorption in the THz range, THz generation in QPM GaAs by parametric down-conversion has been extensively studied [8]. Recently, THz wave generated in periodically-inverted diffusion-bonded GaAs stacks has been demonstrated [9]. To bond the GaAs stacks, processes with a uniform pressure up to

$107N/m^2$ and a temperature up to $1000^{\circ}C$ are required [10]. On the other hand, THz wave generation based on orientation-patterned GaAs crystal has also been reported in some studies [11], which explain that the crystal is grown by the combination of hydride vapor phase epitaxy and molecular beam epitaxy. Although this all-epitaxial growth technique can precisely control the QPM period with a submicron resolution, fabricating the samples with relatively large clear apertures and sufficient thicknesses is difficult.

To achieve a large aperture QPM GaAs without the aforementioned complicated fabrication process, optically contacted GaAs (OC-GaAs) fabricated by simply stacking up 1 mm thick, 2'' in diameter (110) GaAs wafers in a clean room is demonstrated [12]. By pumping along the [110] direction of the GaAs to utilize its maximum $d_{eff}$, THz wave generation is observed. Although the optically contacted wafers can be stacked very closely to each other that the air gap between adjacent layers is smaller than the wavelength of the pump (p), reflection losses from the surfaces and the interfaces limit the number of possible QPM periods. In effect, optically clear interfaces are usually difficult to obtain when the number of QPM periods exceeds five [8]. Therefore, in this paper, we propose a different pumping configuration in generating THz, in which a TM-polarized wave is pumped near the Brewster angle of the OC-GaAs to reduce the reflection loss [13] both from the surfaces and interfaces. Compared with the normal incidence configuration used conventionally, the number of optimal QPM periods of the near-Brewster angle pumped configuration can be increased, and a large overall enhancement in the conversion efficiency can be achieved.

### *A. Simulation results*

Figure 5-3 shows the propagation and polarization configurations of a near-Brewster angle pumped QPM OC-GaAs. In our study, the pump and signal wavelengths at $\lambda_p$ = 3.448 μm and $\lambda_s$ = 3.471 μm are considered because the two wavelengths avoid two-photon absorption in GaAs and are the idler wavelengths of a convenient 1064 nm pumped optical parametric amplification seeded by telecom

diodes [10]. The absorption coefficients of the pump and the THz waves at the corresponding wavelengths are $\alpha_p$ = 0.01 cm$^{-1}$ and $\alpha_{THz}$ = 0.2 cm$^{-1}$ [14], respectively. With a QPM period of 2 mm (1 mm thick wafer), a THz wave at $\lambda_{THz}$ = 515.7 μm can be produced. The refraction indices of the GaAs at the corresponding pump and THz wavelengths are $n_p$ = 3.335 and $n_{THz}$ = 3.6, respectively. To account for the transmission loss between each layer, a normalized air-gap spacing $D/\lambda_p$ between each wafer is considered.

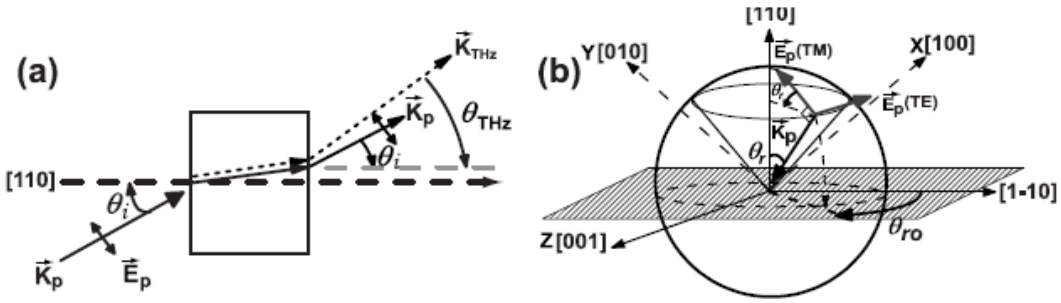


**Fig. 5-3** (a) Propagation and (b) polarization configurations for THz generation in a near-Brewster angle pumped (110) QPM OC-GaAs.

In conventional configurations, a pump wave is incident normally to a QPM GaAs along the [110] axis and polarized in the $[1\,\bar{1}\,1]$ direction to utilize fully its largest nonlinear coefficient $d_{eff} = \frac{2}{\sqrt{3}} d_{14}$ [15, 16]. However, significant reflection losses at the surfaces and interfaces limit the possible number of QPM periods and THz conversion efficiency. Therefore, as Fig. 5-3(a) shows, a TM-polarized pump incident on the QPM OC-GaAs with an angle $\theta_i$ tilted from the [110] axis is utilized to minimize the reflection losses from the surfaces. The pump wave inside the GaAs layer and the generated THz wave transmitted have refraction angles of $\theta_r$ and $\theta_{THz}$, respectively. For a pump wave inside the GaAs with an angle $\theta_r$, it can rotate arbitrarily along the [110] axis within the cone as shown in Fig. 5-3(b), where the rotation angle of its projection on the (110) plane from the $[1\,\bar{1}\,1]$ axis is denoted as $\theta_{ro}$.

For a pump wave incident at $\theta_i$ with a polarization angle $\theta_{ro}$, the projections

of the *E* field at the *x*, *y*, and *z* axes according to Fig. 5-3(b) are as follows:

$$E_x = E\sqrt{1-\cos^2\theta_r \sin^2\theta_{ro}}\,\sin\left[\tan^{-1}\left(\frac{\tan\theta_r}{\cos\theta_{ro}}\right)-\frac{\pi}{4}\right] \quad (1)$$

$$E_y = E\sqrt{1-\cos^2\theta_r \sin^2\theta_{ro}}\,\cos\left[\tan^{-1}\left(\frac{\tan\theta_r}{\cos\theta_{ro}}\right)-\frac{\pi}{4}\right] \quad (2)$$

and

$$E_z = -E\cos(\theta_r)\sin(\theta_{ro}) \quad (3)$$

where $\theta_r = \sin^{-1}\left(\frac{\sin(\theta_i)}{n_p}\right)$. From the nonlinear susceptibility $\chi^{(2)}$ of GaAs, the maximum effective nonlinear coefficients $d_{eff}$ of a TM-polarized pump incident at different $\theta_i$ optimized with rotation angles $\theta_{ro}$ are calculated (see Fig. 5-4[a]), where the maximum $d_{eff}$ is normalized to the nonlinear coefficient $d_{14}$ of GaAs. The optimal rotation angle $\theta_{ro}$ is determined by rotating the pump along the cone described in Fig. 5-3(b) to obtain the largest $d_{eff}$ [17]. As can be seen, $d_{eff}$ decreases as $\theta_i$ increases, an obvious reason for adopting the normal incident pump as in the conventional configuration. However, although the $d_{eff}$ is slightly decreased when compared with the normal incidence case, the TM-polarized pump incident at a tilted angle experiences much less reflection loss from the interfaces; hence it is expected to contribute to the higher overall conversion efficiency when a multiple-layer QPM OC-GaAs structure is used.

Figure 5-4(b) shows the transmission coefficients of the TM-polarized pump wave of the GaAs calculated with different incident angles [18]. As shown in the figure, the total transmission occurs at the Brewster angle of $\theta_i$ = 73.5°, while only 71.25 % can be transmitted for normal incidence. In spite of the higher transmission for the pump wave, the total internal reflection of the THz wave (dashed curve) occurs

when $\theta_i$ > 66.92◦ because of the higher refractive index at the THz wavelength. In effect, to minimize the reflection loss of the pump while still avoiding the total internal reflection of the THz wave generated, pumping at a near-Brewster angle $\theta_i$ =66.92◦ before the total internal reflection occurred is preferred. At $\theta_i$ =66.92◦, a maximum $d_{eff}$ of $0.9014d_{14}$ with $\theta_{r0}$ = 33.58◦ and a transmittance above 97.8% can be achieved. Note that when the incident angle is close to the Brewster angle, coupling the THz wave out from the OC-GaAs can be difficult because of the diffraction of the THz wave. This can be overcome by attaching a GaAs wedge and/or a silicon hemisphere ball-lens (n=3.4) to the last GaAs plate for better out-coupling.

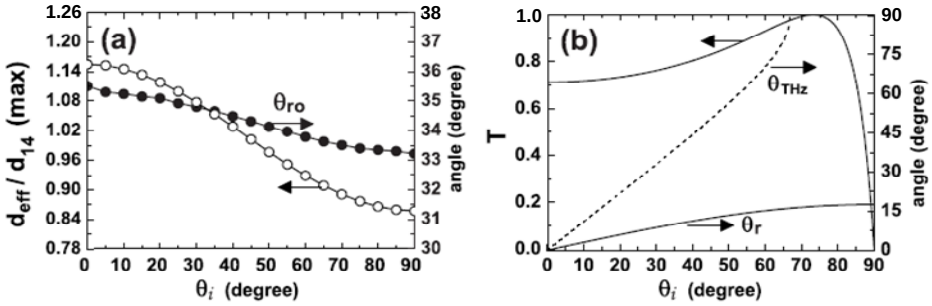


**Fig. 5-4** (a) Maximum $d_{eff}$ and its corresponding polarization direction $\theta_{ro}$ (refer to Fig. 5-3[b]) as a function of $\theta_i$; (b) Transmittance of the TM-polarized pump and refraction angles of the pump ($\theta_r$) and the THz ($\theta_{THz}$) waves for different incidence angles $\theta_i$.

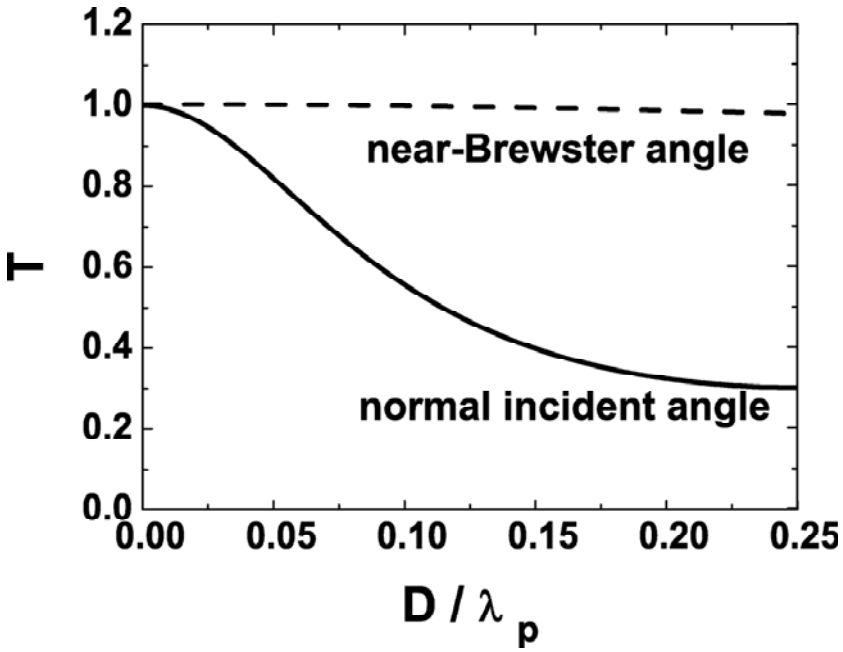


**Fig. 5-5** Transmittances of the pump wave with normal (dashed curve) and near-Brewster angle (solid curve) incidences for different air-gap spacings.

In an OC-GaAs sample, the spacing of the air-gap between each layer affects the transmittance of the pump wave that can propagate into the successive wafers of the QPM structure. Figure 5-5 shows the transmittances of the pump wave at the interface for the normal (dashed curve) and near-Brewster angle ($\theta_i$ = 66.92◦) (solid curve) incidences with different air-gap spacings $D/\lambda_p$, respectively. Apparently, while the transmittance of the pump incident at the near-Brewster angle remains at a high transmission level, the transmittance of the normal incidence case rapidly reduces as $D/\lambda_p$ increases: it drops to its minimum of 0.3 when the spacing is equal to a quarter wavelength of the pump ($D/\lambda_p$ = 0.25) [9, 14]. The significant reflection loss of the pump in the normal incidence case can hamper the overall efficiency of THz generation.

By solving the following coupled equations of the parametric down-conversion [ 19 ] for each successive layer of QPM OC-GaAs with the aforementioned considerations,

$$\frac{dE_p}{dz} + \alpha_p E_p = -j\kappa_p E_s E_{THz} e^{j\Delta kz} \tag{4}$$

$$\frac{dE_s}{dz} + \alpha_s E_s = -j\kappa_s E_p E_{THz}^* e^{-j\Delta kz} \tag{5}$$

and

$$\frac{dE_{THz}}{dz} + \alpha_{THz} E_{THz} = -j\kappa_{THz} E_s E_p^* e^{-j\Delta kz} \tag{6}$$

The efficiencies of the TE- and TM-polarized THz generations with near-Brewster angle pumped QPM OC-GaAs for different numbers of QPM periods under the condition of different air-gap spacings are calculated and shown in Figs. 5-6(a) and (b), respectively. In this calculation, $E$ is the electric field; $\alpha$ is the absorption coefficient; $\kappa$ is the coupling coefficient; $\Delta k$ is the phase mismatch; and the subscripts *s*, *p*, and *THz* denote the signal, pump, and THz waves, respectively. The power of the THz wave generated is normalized to the power of the pump wave, where pulse energies of 10 μJ and 5 μJ for the pump and the signal waves, respectively, with 0.5 ns pulse width are considered. As can be seen, the conversion efficiency of the TE-polarized THz wave is much lower than that in the TM-polarized THz. This is because at $\theta_i = 66.92^\circ$ with $\theta_{ro} = 33.58^\circ$, the maximum $d_{eff}$ occurs at a polarization direction almost perpendicular to the TE polarization. Therefore, the THz conversion takes place only in the direction of the TM polarization. For $D/\lambda_p =$ 0.025 ($D$=85 nm with $\lambda_p$=3.4 μm), the optimal number of QMP periods for the maximum TM-polarized THz conversion is about 25, hence yielding a conversion efficiency of $4.02\times10^{-3}$.

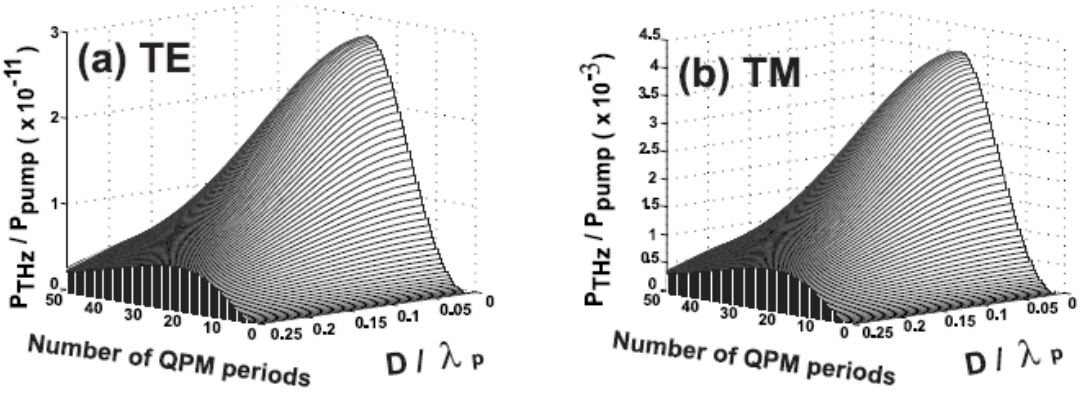


**Fig. 5-6** Efficiencies of the (a) TE- and (b) TM-polarized THz generation for different number of QPM periods and air-gap spacings.

To compare with the benchmark of the normal incidence case, Fig. 5-7 shows the overall (TE- and TM-polarized THz waves combined) efficiency of THz wave generation. As can be seen in Fig. 5-7(a), in the extreme case of no air-gap between the interfaces ($D$ = 0, reflections only occur at the input and output surfaces but not between each layer), the efficiency of the normal incidence case (dashed blue curve) outperforms the near-Brewster angle pumped case (solid blue curve) marginally for QPM periods less than 17 contributing from the higher $d_{eff}$ at $\theta_i$=0◦. On the contrary, because of the minimized reflection losses on the input and output surfaces, the near-Brewster angle pumped case does not reach its maximum of $4.07\times10^{-3}$ until QPM periods of 25 are reached. As a result, with a higher pump power reaching into the QPM OC-GaAs, the efficiency of the near-Brewster angle pumped case eventually surpasses the normal incidence case if an optimized number of QPM periods is chosen.

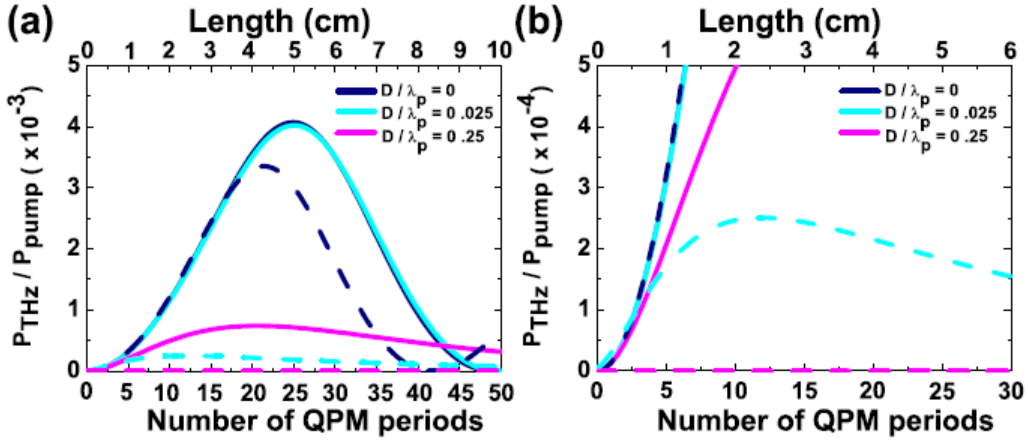


**Fig. 5-7** (Color online) (a) Efficiencies of the THz generation versus the number of QPM periods with the near-Brewster angle (solid curves) and the normal incidence (dashed curves) cases, where the blue, cyan, and magenta curves are for cases of $D/\lambda_p$ = 0, $D/\lambda_p$ = 0.25, and $D/\lambda_p$ = 0.025, respectively; (b) Zoom image of the low-efficiency region of Fig. 5(a) to show the details of the normal incidence case.

Nonetheless, air-gaps in the interfaces inevitably exist. In the case of $D/\lambda_p$=0.025, for example, the efficiencies of the near-Brewster angle pumped case and the normal incidence case are shown in Fig. 5-7(a) with the solid cyan and dashed cyan curves, respectively. Figure 5-7(b) zooms in on the low-efficiency region of Fig. 5-7(a) to show the details of the normal incidence case. Considering the air-gap, which introduces the reflection loss of the pump wave before entering the successive layer, the efficiency of the normal incidence case drops severely compared with the near-Brewster angle pump case. Suffering from a great loss in the reflection, the normal incidence case reaches its maximum efficiency of only $0.251\times10^{-3}$ at QPM periods of 12. At the same time, by simply changing the incident angle of the pump to the near-Brewster angle $\theta_i$=66.92◦, a gain of 6 times can be obtained with the same number of QPM periods. With the possibility of increasing the QPM periods to 25, a gain of more than 16 times for the near-Brewster angle case can eventually be reached.

### *B. Summary*

In summary, the advantages of pumping a QPM OC-GaAs sample with the

TM-polarized pump incident at a near-Brewster angle is discussed and studied. Although the effective nonlinear coefficient may be slightly lower compared with the normal incidence case, significantly reducing the reflection losses on both the surfaces and interfaces enhances not only the possibility of increasing the QPM periods but also benefits the overall conversion efficiency. Under the near-Brewster angle pumping configuration studied, the QPM OC-GaAs is a promising device for efficient THz wave generation because it has the following advantages: high conversion efficiency, large aperture, and better yet easy fabrication process.

## References


1 M. Schall, H. Helm, S.R. Keiding, “Far infrared properties of electro-optic crystals measured by THz time-domain spectroscopy,” Int. J. Infrared and MM Waves **20**, 595-604 (1999).

2 J. A. Armstrong, N. Bloemergen, J. Ducuing, and P. S. Pershan, “Interactions between light waves in a nonlinear dielectric,” Phys. Rev., **127**, 1918-1939 (1962).

3 A. C. Chiang, T. D. Wang, Y. Y. Lin, S. T. Lin, H. H. Lee, Y. C. Huang, and Y. H. Chen, “Enhanced terahertz-wave parametric generation and oscillation in lithium niobate waveguides at terahertz frequencies,” Opt. Lett. **30**, 3392-3394 (2005).

4 Y. Takushima, S. Y. Shin, and Y. C. Chung, “Design of a $LiNbO_3$ ribbon waveguide for efficient difference-frequency generation of terahertz wave in the collinear configuration,” Opt .Express **14**, 14783-14792 (2007).

5 P. H. Siegel, ”Terahertz technology in biology and medicine,” IEEE T. Microw. Theory **52**, 2438-2447 (2004).

6 H. Feng, F. John, G. Dale, B. Robert, and Z. David, ”Noninvasive study of explosive materials by time domain spectroscopy and FTIR,” in AIP conference proceedings **760**, 578-585(2005).

7 T. Kleine-Ostmann, K. Pierz, G. Hein, P. Dawson, and M. Koch, ”Audio signal transmission over THz communication channel using semiconductor modulator,” Electron. Lett. **40**, 124-126 (2004).

8 G. Imeshev, M. E. Fermann, K. L. Vodopyanov, M. M. Fejer, X. Yu, J. S. Harris, D. Bliss, and C. Lynch, ”High-power source of THz radiation based on orientation-patterned GaAs pumped by a fiber laser,” Opt .Express **14**, 4439-4444 (2006).

9 Y. S. Lee, W. C. Hurlbut, K. L. Vodopyanov, M. M. Fejer,and V. G. Kozlov, ”Coherent detection of multi-cycle terahertz pulses generated in periodically inverted GaAs structures,” Proc. SPIE **6455**, 64550G (2007).

10 D. Zheng, ”Tunable infrared generation with diffusion-bonded-stacked gallium arsenide,” PhD thesis, Stanford University GL8900 (1998).

11 K. L. Vodopyanov, M. M. Fejer, X. Yu, J. S. Harris, Y. S. Lee, W. C. Hurlbut, V. G. Kozlov, D. Bliss, and C.Lynch, ”Terahertz-wave generation in quasi-phase-matched GaAs,” Appl. Phys. Lett. **89**, 141119 (2006).

12 Y. S. Lee, W. C. Hurlbut, K. L. Vodopyanov, M. M. Fejer, and V. G. Kozlov, ”Generation of multicycle terahertz pulses via optical rectification in periodically inverted GaAs structures,” Appl. Phys. Lett. **89**, 181104 (2006).

13 A. Szilagyi, A. Hordvik, and H. Schlossberg, ”A quasi-phase-matching technique for efficient optical mixing and frequency doubling,” J. of Appl. Phys. **47**, 2025-2032 (1976).

14 D. Grischkowsky, S. Keiding, M. van Exter, and C. Fattinger, ”Far-infrared

time-domain spectroscopy with terahertz beams of dielectrics and semiconductors," J. Opt. Soc. Am. B **7**, 2006-2015 (1990).

15 K. L. Vodopyanov, O. Levi, P. S. Kuo, T. J. Pinguet, J. S. Harris, and M. M. Fejer, "Optical parametric oscillation in quasi-phase-matched GaAs, " Opt. Lett. **29**, 1912-1914 (2004).

16 Q. Chen, M. Tani, Z. Jiang, and X. C. Zhang, "Electro-optic transceivers for terahertz-wave applications," J. Opt. Soc. Am B **18**, 823-831 (2001).

17 B. Wyncke and F. Brehat, "Calculation of the effective second-order non-linear coefficients along the phase matching directions in a centric orthorhombic biaxial crystals," J. of Phys. B: At. Mol. Opt. Phys. **22**, 363-376 (1989).

18 E. Hecht, *Optics*, 4th ed. (Academic, Adelphi, 2002).

19 X. Liu and H. Zhang, "Exact analytical solutions and their applications for interacting waves in quadratic nonlinear medium," Opt. Express **10**, 83-97 (2002).

# List of Publications

## A. International journal papers

1. A. C. Chiang, Y. Y. Lin, T. D. Wang, Y. C. Huang, and J. T. Shy, "Distributed feedback optical parametric oscillation by use of a photorefractive grating in periodically-poled lithium niobate," Optics Letters **27**, 1815-1818 (2002) .
2. A. C. Chiang, T. D. Wang, Y. Y. Lin, C. W. Liu, Y. H. Chen, B. C. Wong, and Y. C. Huang, "Pulsed optical parametric generation, amplification and oscillation in monolithic PPLN crystals," IEEE J. Quan. Elec. **40**, 791-799 (June, 2004).
3. A. C. Chiang, T. D. Wang, Y. Y. Lin, S. T. Lin, H. H. Lee, and Y. C. Huang, "Enhanced terahertz-wave parametric generation and oscillation in lithium niobate waveguides at terahertz wavelength," Optics Letters **27**, 1815-1818 (2005) .
4. F. Y. Lin, H. L. Lu, T. D. Wang, Y. C. Huang, "High-efficiency THz generation in optically-contacted GaAs with near–Brewster angle pumping," Optics Express, vol. **15**, 13654-13659 (2007).
5. T. D. Wang, S. T. Lin, Y. Y. Lin, A. C. Chiang, and Y. C. Huang, "Forward and backward THz-wave generations from periodically poled lithium niobate," Optics Express **16**, 6471-5478 (2008).
6. T. D. Wang, Y. Y. Lin, S. Y. Chen, A. C. Chiang, S. T. Lin, and Y. C. Huang, "Low-threshold, narrow-line THz-wave parametric oscillator with an intra-cavity grazing-incidence grating ," Optics Express **16**, 12571-12576 (2008).
7. Y. C. Huang, A. S. Solntsev, T. D. Wang, W. W. Hsu, " Generation of fs laser pulses from a ps pulse-pumped optical parametric amplifier with a beat-wave seed signal," Optics Communications **282**, 2250-2254 (2009).

## B. International Conference Papers

1. Yen-Chieh Huang, Tsong-Dong Wang, An-Chung Chiang , Heng-Sheng Lee, "Waveguide-Enhanced THz Parametric Generation and Oscillation in Thin Lithium Niobate Wafer," CLEO-USA 2005 (CTuBB2, oral presentation),

Baltimore, May 22-27, 2005 .

2. T. D. Wang, H. L. Chang, A. C. Chiang, Y. C. Huang, "Narrow-line, high-repetition-rate THz-wave Generation from Collinearly Phase-matched Periodically Poled Lithium Niobate," OSA Topic Meeting: Optic al THz Science and Technology, March 18-21, 2007, Orlando, Florida, USA.
3. T. D. Wang, H. L. Chang, S. T. Lin, Y. Y. Lin, A. C. Chiang, and Y. C. Huang, "Narrow-Line, High-Repetition-Rate THz-Wave Generation from Collinearly Phase-Matched Difference-Frequency Mixing in Periodically Poled Lithium Niobate," CLEO2007 (JWA98), May 6-11, 2007, Baltimore, Maryland, USA.
4. T. D. Wang, H. L. Chang, S. T. Lin, Y. Y. Lin, A. C. Chiang, and Y. C. Huang, "Backward THz-wave Generation from Collinearly Phase-Matched Difference-Frequency Mixing in Periodically Poled Lithium Niobate," CLEO2008 (CFV5), May 4-9, 2008, San Jose, California, USA.
5. Yen-Yin Lin, R. Y. Tu, T. D. Wang, S. T. Lin, A. C. Chiang, Y. H. Chen, Y. C. Huang, "Watt-Level Single-Longitudinal-Mode, Tunable Dual-Wavelength, CW Nd:YVO4 Laser," CLEO2008 (CFJ3), May 4-9, 2008, San Jose, California, USA.
6. Yen-Chieh Huang, Tsong-Dong Wang, Wei-Chen Cheng, "Beat-Wave-Seeded, Pulsed Optical Parametric Amplifier," CLEO2008 (CWC3), May 4-9, 2008, San Jose, California, USA.
7. T. D. Wang, S. T. Lin, Y. Y. Lin, F. Y. Lin, and Y. C. Huang, "Backward Terahertz-wave difference-frequency generation from periodically poled lithium niobate," OPT2008, poster presentation QO-010, Taipei, Dec. 2008.
8. Tsong-Dong Wang, S. T. Lin, Y. Y. Lin, F. Y. Lin, Y. C. Huang, "Forward and Backward Terahertz-Wave Difference-Frequency Generations from Periodically Poled Lithium Niobate," ASSP2009 (TuC5), Feb.1-4, 2009, Denver, Colorado, USA.
9. Shoutai Lin, Yen-Yin Lin, Rong-Yu Tu, Tsong-Dong Wang, Yen-Chieh Huang, "Fiber-Laser-Pumped CW OPO for Red, Green, Blue Laser Generation," CLEO 2009 (CWJ4), May 31-June 5, 2009, Baltimore, Maryland, USA.
10. Rong-Yu Tu, Yen-Yin Lin, Shou-Tai Lin, Tsong-Dong Wang, Chin-Yuan Chien, Yen-Chieh Huang, "Sodium-Yellow Laser Generation from a Three-Stage $\chi^{(2)}$

Process in an Optical Parametric Oscillator," CLEO 2009 (JWA10), May 31-June 5, 2009, Baltimore, Maryland, USA.

11. An-Chung Chiang, Y. Y. Lin, S. T. Lin, T. D. Wang, Y. C. Huang, "A compact and wavelength-tunable PPLN EO Q-switch laser with intra-cavity optical parametric generation," NLO 2009 (NThB1), July 12-17, 2009, Honolulu, Hawaii, USA.
12. Tsong-Dong Wang, S. T. Lin, Y. Y. Lin, F. Y. Lin, Y. C. Huang, "Forward and Backward Terahertz-Wave Difference-Frequency Generations from Periodically Poled Lithium Niobate," CLEO / Pacific Ring 2009 (CLEO-2009-919), Aug.30-Sep.3, 2009, Shanghai, China.

## C. Domestic Conference Papers

1. 王寵棟、梁雲清、蔣安忠、陳彥宏、林子加、黃衍介、施宙聰、陳永富、曹培熙, "雙重路徑準相位匹配鈮酸鋰光參數產生器與窄頻寬光參數放大器," OPT2001, National Sun Yat-Sen University, Kaohsiung, Taiwan, Dec. 13-14, 2001.
2. A. C. Chiang, T. D. Wang, T. C. Lin, B. C. Wong, J. T. Shy and Y. C. Huang, "Distributed Feedback Optical Parametric Oscillator in Periodically-Poled Lithium Niobate," Proceedings First Taiwan Symposium on Novel Nonlinear Optical Materials and Quasi-phase-matched Laser Devices, Oct. 25-26, 2001, National Tsinghua University, Hsinchu, Taiwan.
3. T. D. Wang, A. C. Chiang, T. C. Lin, B. C. Wong, and Y. C. Huang," TEMPORAL AND SPECTRAL EXPERIMENT FOR MUTIPLE-PASS, ULTRAL-LOW-THRESHOLD OPTICAL PARAMETRIC GENERAION FROM PPLN, " Proceedings First Taiwan Symposium on Novel Nonlinear Optical Materials and Quasi-phase-matched Laser Devices, Oct. 25-26, 2001, National Tsinghua University, Hsinchu, Taiwan.
4. A. C. Chiang, Y. Y. Lin, T. D. Wang , J. T. Shy and Y. C. Huang, "Nonlinear wave mixing in a periodic nanostructure for short-wavelength laser generation," Proceedings APAM 2002 International Conference on International Collaboration and Networking: Creating a Global nanotechnology Network, Dec. 9-11, 2002, National Tsinghua University, Hsinchu, Taiwan.

5. C. K. Lakshmana Perumal, Y. Y. Lin, T. D. Wang, P. Santhana Raghavan, P.Ramasamy and Y.C. Huang, “Crystal Growth of Nonlinear Optical Crystal 4-MethoxyBenzaldehyde-N-methyl –4-Stilbazolium Tosylate (MBST) and their characterization,” OPT2001, National Sun Yat-Sen University, Kaoshiung, Taiwan, Dec. 13-14, 2001.
6. Y. Y. Lin, C. K. Lakshmana Perumal, T. D. Wang, , P. Santhana Raghavan, P. Ramasamy and Y. C. Huang, “CRYSTAL GROWTH AND NLO CHARACTERIZATION OF MHB CRYSTALS,” Proceedings First Taiwan Symposium on Novel Nonlinear Optical Materials and Quasi-phase-matched Laser Devices, Oct. 25-26, 2001, National Tsinghua University, Hsinchu, Taiwan.
7. T. D. Wang, R. Y. Tu, Y. Y. Lai, H. H. Lee, A. C. Chiang, Y. H. Chen, and Y. C. Huang, “HIGH-EFFICIENCY NON-COLLINEARLY PHASE-MATCHED THZ PARAMETRIC GENERATION AND OSCILLATION IN LITHIUM NIOBATE WAVEGUIDES,” OPT2004, paper C1N-4681, National Centarl University, Taoyuan, Taiwan, Dec. 18-19, 2004.
8. S. I. Chen, R. Y. Tu, T. D. Wang, A. C. Chiang, Y. Y. Lin, S. T. Lin, Y. H. Chen and Y. C. Huang, “INJECTION SEEDING NARROW LINEWIDTH HIGH-EFFICIENCY NON-COLLINEARLY PHASE-MATCHED THZ PARAMETRIC GENERATION AND OSCILLATION IN LITHIUM NIOBATE WAVEGUIDES,” OPT2005, National Chen-Kung University, Kaohsiung, Taiwan, Dec. 09-10, 2005.
9. T. D. Wang, H. L. Chang, H. L. Lu, S. T. Lin, Y. Y. Lin, A. C. Chiang, F. Y. Lin, and Y. C. Huang, “HIGH-REPETITION AND NARROW-BANDWIDTH TERAHERTZ-WAVE DIFFERENCE-FREQUENCY GENERATION IN PERIODICALLY POLED LITHIUM NIOBATE,” OPT2006, National Tsinghua University, Hsinchu, Taiwan, Dec. 15-16, 2005.
10. H. L. Lu, J. H. Chen, T. D. Wang, Y. C. Huang, and F. Y. Lin, "High-efficiency THz generation in optically contacted GaAs with near Brewster angle pumping," in OPT 2007, Taichung, Taiwan, 2007.

## D. Domestic Technical Papers

1. 陳彥宏、蔣安忠、張可為、王寵棟、鄒德皓、林子加、李穎玟、黃衍介, “準相位匹配鈮酸鋰雷射波長轉換,” 光訊第 93 期第 23 頁及第 94 期(2001)。
2. 王寵棟、黃衍介, “在週期性極化鈮酸鋰晶體中利用雷射差頻產生正向與反向的同調性兆赫波幅射,” 物理雙月刊第 31 卷第 2 期第 145-150 頁(2009 年四月)。

## E. Award and Honor

1. 清華大學國際訪問獎, 2007
2. 台灣光電科技研討會 OPT2008 壁報論文獎（此次為國際會議）
3. Advanced Solid State Photonics Conference Student Presentation-Travel Award (2009)

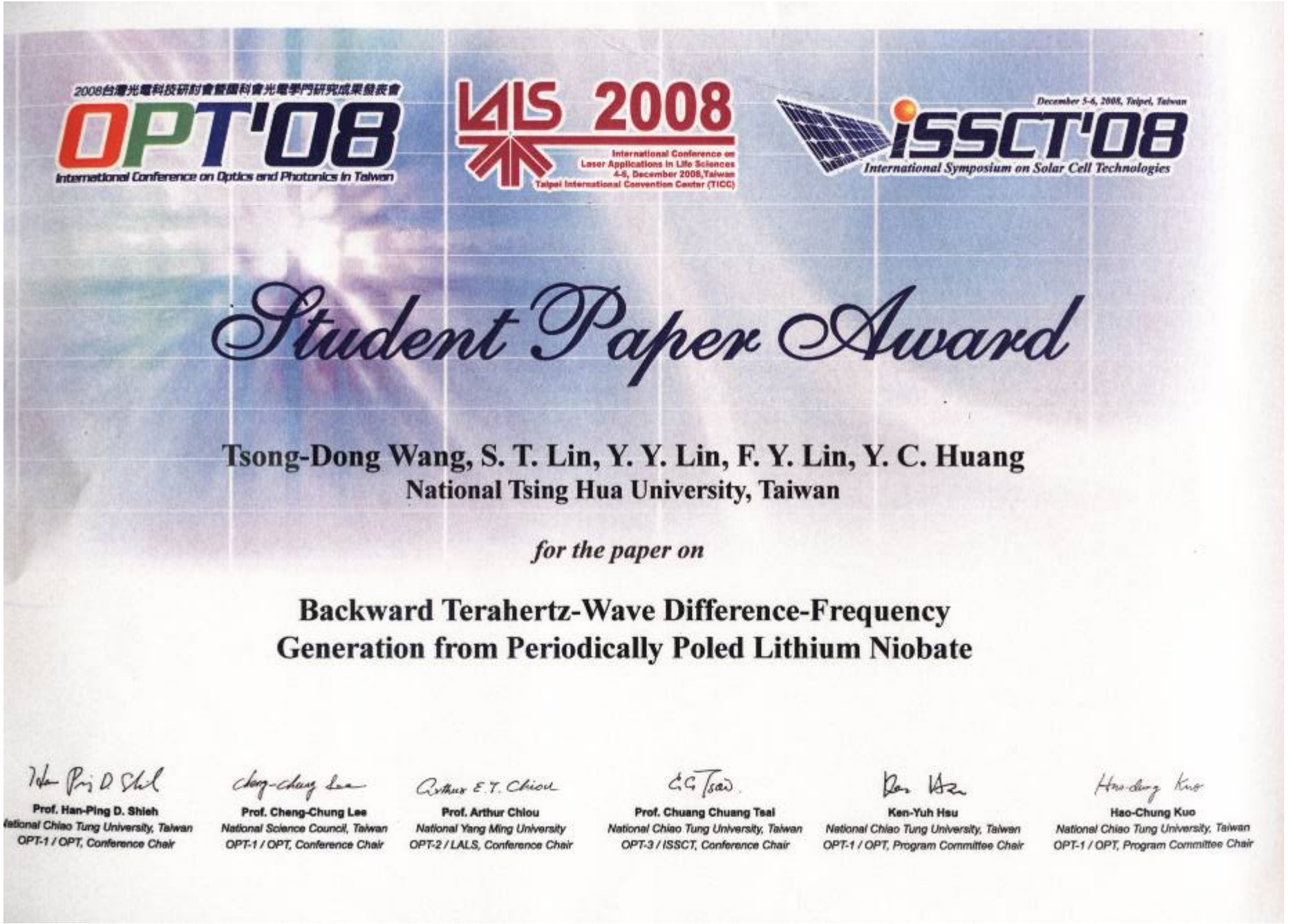
2008台灣光電科技研討會暨國科會光電學門研究成果發表會
OPT'08
International Conference on Optics and Photonics in Taiwan
LALS 2008
International Conference on Laser Applications in Life Sciences
4-6, December 2008,Taiwan
Taipei International Convention Center (TICC)
December 5-6, 2008, Taipei, Taiwan
iSSCT'08
International Symposium on Solar Cell Technologies
Student Paper Award
Tsong-Dong Wang, S. T. Lin, Y. Y. Lin, F. Y. Lin, Y. C. Huang
National Tsing Hua University, Taiwan
for the paper on
Backward Terahertz-Wave Difference-Frequency Generation from Periodically Poled Lithium Niobate
Prof. Han-Ping D. Shieh
National Chiao Tung University, Taiwan
OPT-1 / OPT, Conference Chair
Prof. Cheng-Chung Lee
National Science Council, Taiwan
OPT-1 / OPT, Conference Chair
Prof. Arthur Chiou
National Yang Ming University
OPT-2 / LALS, Conference Chair
Prof. Chuang Chuang Tsai
National Chiao Tung University, Taiwan
OPT-3 / ISSCT, Conference Chair
Ken-Yuh Hsu
National Chiao Tung University, Taiwan
OPT-1 / OPT, Program Committee Chair
Hao-Chung Kuo
National Chiao Tung University, Taiwan
OPT-1 / OPT, Program Committee Chair